Measurement of the semileptonic charge asymmetry in B^0 meson mixing with the D0 detector

V. M. Abazov,[32] B. Abbott,[68] B. S. Acharya,[26] M. Adams,[46] T. Adams,[44] G. D. Alexeev,[32] G. Alkhazov,[36] A. Alton,[57,*] A. Askew,[44] S. Atkins,[55] K. Augsten,[7] C. Avila,[5] F. Badaud,[10] L. Bagby,[45] B. Baldin,[45] D. V. Bandurin,[44] S. Banerjee,[26] E. Barberis,[56] P. Baringer,[53] J. F. Bartlett,[45] U. Bassler,[15] V. Bazterra,[46] A. Bean,[53] M. Begalli,[2] L. Bellantoni,[45] S. B. Beri,[24] G. Bernardi,[14] R. Bernhard,[19] I. Bertram,[39] M. Besançon,[15] R. Beuselinck,[40] P. C. Bhat,[45] S. Bhatia,[59] V. Bhatnagar,[24] G. Blazey,[47] S. Blessing,[44] K. Bloom,[60] A. Boehnlein,[45] D. Boline,[65] E. E. Boos,[34] G. Borissov,[39] A. Brandt,[71] O. Brandt,[20] R. Brock,[58] A. Bross,[45] D. Brown,[14] J. Brown,[14] X. B. Bu,[45] M. Buehler,[45] V. Buescher,[21] V. Bunichev,[34] S. Burdin,[39,†] C. P. Buszello,[38] E. Camacho-Pérez,[29] B. C. K. Casey,[45] H. Castilla-Valdez,[29] S. Caughron,[58] S. Chakrabarti,[65] D. Chakraborty,[47] K. M. Chan,[51] A. Chandra,[73] E. Chapon,[15] G. Chen,[53] S. Chevalier-Théry,[15] S. W. Cho,[28] S. Choi,[28] B. Choudhary,[25] S. Cihangir,[45] D. Claes,[60] J. Clutter,[53] M. Cooke,[45] W. E. Cooper,[45] M. Corcoran,[73] F. Couderc,[15] M.-C. Cousinou,[12] A. Croc,[15] D. Cutts,[70] A. Das,[42] G. Davies,[40] S. J. de Jong,[30,31] E. De La Cruz-Burelo,[29] F. Déliot,[15] R. Demina,[64] D. Denisov,[45] S. P. Denisov,[35] S. Desai,[45] C. Deterre,[15] K. DeVaughan,[60] H. T. Diehl,[45] M. Diesburg,[45] P. F. Ding,[41] A. Dominguez,[60] A. Dubey,[25] L. V. Dudko,[34] D. Duggan,[61] A. Duperrin,[12] S. Dutt,[24] A. Dyshkant,[47] M. Eads,[60] D. Edmunds,[58] J. Ellison,[43] V. D. Elvira,[45] Y. Enari,[14] H. Evans,[49] A. Evdokimov,[66] V. N. Evdokimov,[35] G. Facini,[56] L. Feng,[47] T. Ferbel,[64] F. Fiedler,[21] F. Filthaut,[30,31] W. Fisher,[58] H. E. Fisk,[45] M. Fortner,[47] H. Fox,[39] S. Fuess,[45] A. Garcia-Bellido,[64] J. A. García-González,[29] G. A. García-Guerra,[29,‡] V. Gavrilov,[33] P. Gay,[10] W. Geng,[12,58] D. Gerbaudo,[62] C. E. Gerber,[46] Y. Gershtein,[61] G. Ginther,[45,64] G. Golovanov,[32] A. Goussiou,[75] P. D. Grannis,[65] S. Greder,[16] H. Greenlee,[45] G. Grenier,[17] Ph. Gris,[10] J.-F. Grivaz,[13] A. Grohsjean,[15,§] S. Grünendahl,[45] M. W. Grünewald,[27] T. Guillemin,[13] G. Gutierrez,[45] P. Gutierrez,[68] J. Haley,[56] L. Han,[4] K. Harder,[41] A. Harel,[64] J. M. Hauptman,[52] J. Hays,[40] T. Head,[41] T. Hebbeker,[18] D. Hedin,[47] H. Hegab,[69] A. P. Heinson,[43] U. Heintz,[70] C. Hensel,[20] I. Heredia-De La Cruz,[29] K. Herner,[57] G. Hesketh,[41,¶] M. D. Hildreth,[51] R. Hirosky,[74] T. Hoang,[44] J. D. Hobbs,[65] B. Hoeneisen,[9] J. Hogan,[73] M. Hohlfeld,[21] I. Howley,[71] Z. Hubacek,[7,15] V. Hynek,[7] I. Iashvili,[63] Y. Ilchenko,[72] R. Illingworth,[45] A. S. Ito,[45] S. Jabeen,[70] M. Jaffré,[13] A. Jayasinghe,[68] M. S. Jeong,[28] R. Jesik,[40] P. Jiang,[4] K. Johns,[42] E. Johnson,[58] M. Johnson,[45] A. Jonckheere,[45] P. Jonsson,[40] J. Joshi,[43] A. W. Jung,[45] A. Juste,[37] E. Kajfasz,[12] D. Karmanov,[34] P. A. Kasper,[45] I. Katsanos,[60] R. Kehoe,[72] S. Kermiche,[12] N. Khalatyan,[45] A. Khanov,[69] A. Kharchilava,[63] Y. N. Kharzheev,[32] I. Kiselevich,[33] J. M. Kohli,[24] A. V. Kozelov,[35] J. Kraus,[59] A. Kumar,[63] A. Kupco,[8] T. Kurča,[17] V. A. Kuzmin,[34] S. Lammers,[49] G. Landsberg,[70] P. Lebrun,[17] H. S. Lee,[28] S. W. Lee,[52] W. M. Lee,[45] X. Lei,[42] J. Lellouch,[14] D. Li,[14] H. Li,[11] L. Li,[43] Q. Z. Li,[45] J. K. Lim,[28] D. Lincoln,[45] J. Linnemann,[58] V. V. Lipaev,[35] R. Lipton,[45] H. Liu,[72] Y. Liu,[4] A. Lobodenko,[36] M. Lokajicek,[8] R. Lopes de Sa,[65] H. J. Lubatti,[75] R. Luna-Garcia,[29,**] A. L. Lyon,[45] A. K. A. Maciel,[1] R. Madar,[19] R. Magaña-Villalba,[29] S. Malik,[60] V. L. Malyshev,[32] Y. Maravin,[54] J. Martínez-Ortega,[29] R. McCarthy,[65] C. L. McGivern,[41] M. M. Meijer,[30,31] A. Melnitchouk,[45] D. Menezes,[47] P. G. Mercadante,[3] M. Merkin,[34] A. Meyer,[18] J. Meyer,[20] F. Miconi,[16] N. K. Mondal,[26] M. Mulhearn,[74] E. Nagy,[12] M. Naimuddin,[25] M. Narain,[70] R. Nayyar,[42] H. A. Neal,[57] J. P. Negret,[5] P. Neustroev,[36] H. T. Nguyen,[74] T. Nunnemann,[22] J. Orduna,[73] N. Osman,[12] J. Osta,[51] M. Padilla,[43] A. Pal,[71] N. Parashar,[50] V. Parihar,[70] S. K. Park,[28] R. Partridge,[70,‖] N. Parua,[49] A. Patwa,[66] B. Penning,[45] M. Perfilov,[34] Y. Peters,[20] K. Petridis,[41] G. Petrillo,[64] P. Pétroff,[13] M.-A. Pleier,[66] P. L. M. Podesta-Lerma,[29,††] V. M. Podstavkov,[45] A. V. Popov,[35] M. Prewitt,[73] D. Price,[49] N. Prokopenko,[35] J. Qian,[57] A. Quadt,[20] B. Quinn,[59] M. S. Rangel,[1] K. Ranjan,[25] P. N. Ratoff,[39] I. Razumov,[35] P. Renkel,[72] I. Ripp-Baudot,[16] F. Rizatdinova,[69] M. Rominsky,[45] A. Ross,[39] C. Royon,[15] P. Rubinov,[45] R. Ruchti,[51] G. Sajot,[11] P. Salcido,[47] A. Sánchez-Hernández,[29] M. P. Sanders,[22] A. S. Santos,[1,‡‡] G. Savage,[45] L. Sawyer,[55] T. Scanlon,[40] R. D. Schamberger,[65] Y. Scheglov,[36] H. Schellman,[48] C. Schwanenberger,[41] R. Schwienhorst,[58] J. Sekaric,[53] H. Severini,[68] E. Shabalina,[20] V. Shary,[15] S. Shaw,[58] A. A. Shchukin,[35] R. K. Shivpuri,[25] V. Simak,[7] P. Skubic,[68] P. Slattery,[64] D. Smirnov,[51] K. J. Smith,[63] G. R. Snow,[60] J. Snow,[67] S. Snyder,[66] S. Söldner-Rembold,[41] L. Sonnenschein,[18] K. Soustruznik,[6] J. Stark,[11] D. A. Stoyanova,[35] M. Strauss,[68] L. Suter,[41] P. Svoisky,[68] M. Titov,[15] V. V. Tokmenin,[32] Y.-T. Tsai,[64] K. Tschann-Grimm,[65] D. Tsybychev,[65] B. Tuchming,[15] C. Tully,[62] L. Uvarov,[36] S. Uvarov,[36] S. Uzunyan,[47] R. Van Kooten,[49] W. M. van Leeuwen,[30] N. Varelas,[46] E. W. Varnes,[42] I. A. Vasilyev,[35] P. Verdier,[17] A. Y. Verkheev,[32] L. S. Vertogradov,[32] M. Verzocchi,[45] M. Vesterinen,[41] D. Vilanova,[15] P. Vokac,[7] H. D. Wahl,[44] M. H. L. S. Wang,[45] J. Warchol,[51] G. Watts,[75] M. Wayne,[51] J. Weichert,[21] L. Welty-Rieger,[48] A. White,[71] D. Wicke,[23] M. R. J. Williams,[39] G. W. Wilson,[53] M. Wobisch,[55] D. R. Wood,[56] T. R. Wyatt,[41] Y. Xie,[45] R. Yamada,[45] S. Yang,[4] T. Yasuda,[45] Y. A. Yatsunenko,[32] W. Ye,[65] Z. Ye,[45] H. Yin,[45] K. Yip,[66] S. W. Youn,[45] J. M. Yu,[57] J. Zennamo,[63] T. Zhao,[75] T. G. Zhao,[41] B. Zhou,[57] J. Zhu,[57] M. Zielinski,[64] D. Zieminska,[49] and L. Zivkovic[70]

(The D0 Collaboration)*

[1]*LAFEX, Centro Brasileiro de Pesquisas Físicas, Rio de Janeiro, Brazil*
[2]*Universidade do Estado do Rio de Janeiro, Rio de Janeiro, Brazil*
[3]*Universidade Federal do ABC, Santo André, Brazil*
[4]*University of Science and Technology of China, Hefei, People's Republic of China*
[5]*Universidad de los Andes, Bogotá, Colombia*
[6]*Charles University, Faculty of Mathematics and Physics, Center for Particle Physics, Prague, Czech Republic*
[7]*Czech Technical University in Prague, Prague, Czech Republic*
[8]*Center for Particle Physics, Institute of Physics, Academy of Sciences of the Czech Republic, Prague, Czech Republic*
[9]*Universidad San Francisco de Quito, Quito, Ecuador*
[10]*LPC, Université Blaise Pascal, CNRS/IN2P3, Clermont, France*
[11]*LPSC, Université Joseph Fourier Grenoble 1, CNRS/IN2P3, Institut National Polytechnique de Grenoble, Grenoble, France*
[12]*CPPM, Aix-Marseille Université, CNRS/IN2P3, Marseille, France*
[13]*LAL, Université Paris-Sud, CNRS/IN2P3, Orsay, France*
[14]*LPNHE, Universités Paris VI and VII, CNRS/IN2P3, Paris, France*
[15]*CEA, Irfu, SPP, Saclay, France*
[16]*IPHC, Université de Strasbourg, CNRS/IN2P3, Strasbourg, France*
[17]*IPNL, Université Lyon 1, CNRS/IN2P3, Villeurbanne, France and Université de Lyon, Lyon, France*
[18]*III. Physikalisches Institut A, RWTH Aachen University, Aachen, Germany*
[19]*Physikalisches Institut, Universität Freiburg, Freiburg, Germany*
[20]*II. Physikalisches Institut, Georg-August-Universität Göttingen, Göttingen, Germany*
[21]*Institut für Physik, Universität Mainz, Mainz, Germany*
[22]*Ludwig-Maximilians-Universität München, München, Germany*
[23]*Fachbereich Physik, Bergische Universität Wuppertal, Wuppertal, Germany*
[24]*Panjab University, Chandigarh, India*
[25]*Delhi University, Delhi, India*
[26]*Tata Institute of Fundamental Research, Mumbai, India*
[27]*University College Dublin, Dublin, Ireland*
[28]*Korea Detector Laboratory, Korea University, Seoul, Korea*
[29]*CINVESTAV, Mexico City, Mexico*
[30]*Nikhef, Science Park, Amsterdam, The Netherlands*
[31]*Radboud University Nijmegen, Nijmegen, The Netherlands*
[32]*Joint Institute for Nuclear Research, Dubna, Russia*
[33]*Institute for Theoretical and Experimental Physics, Moscow, Russia*
[34]*Moscow State University, Moscow, Russia*
[35]*Institute for High Energy Physics, Protvino, Russia*
[36]*Petersburg Nuclear Physics Institute, St. Petersburg, Russia*
[37]*Institució Catalana de Recerca i Estudis Avançats (ICREA) and Institut de Física d'Altes Energies (IFAE), Barcelona, Spain*
[38]*Uppsala University, Uppsala, Sweden*
[39]*Lancaster University, Lancaster LA1 4YB, United Kingdom*
[40]*Imperial College London, London SW7 2AZ, United Kingdom*
[41]*The University of Manchester, Manchester M13 9PL, United Kingdom*
[42]*University of Arizona, Tucson, Arizona 85721, USA*
[43]*University of California Riverside, Riverside, California 92521, USA*
[44]*Florida State University, Tallahassee, Florida 32306, USA*
[45]*Fermi National Accelerator Laboratory, Batavia, Illinois 60510, USA*
[46]*University of Illinois at Chicago, Chicago, Illinois 60607, USA*
[47]*Northern Illinois University, DeKalb, Illinois 60115, USA*
[48]*Northwestern University, Evanston, Illinois 60208, USA*
[49]*Indiana University, Bloomington, Indiana 47405, USA*
[50]*Purdue University Calumet, Hammond, Indiana 46323, USA*
[51]*University of Notre Dame, Notre Dame, Indiana 46556, USA*
[52]*Iowa State University, Ames, Iowa 50011, USA*
[53]*University of Kansas, Lawrence, Kansas 66045, USA*
[54]*Kansas State University, Manhattan, Kansas 66506, USA*
[55]*Louisiana Tech University, Ruston, Louisiana 71272, USA*

[56]Northeastern University, Boston, Massachusetts 02115, USA
[57]University of Michigan, Ann Arbor, Michigan 48109, USA
[58]Michigan State University, East Lansing, Michigan 48824, USA
[59]University of Mississippi, University, Mississippi 38677, USA
[60]University of Nebraska, Lincoln, Nebraska 68588, USA
[61]Rutgers University, Piscataway, New Jersey 08855, USA
[62]Princeton University, Princeton, New Jersey 08544, USA
[63]State University of New York, Buffalo, New York 14260, USA
[64]University of Rochester, Rochester, New York 14627, USA
[65]State University of New York, Stony Brook, New York 11794, USA
[66]Brookhaven National Laboratory, Upton, New York 11973, USA
[67]Langston University, Langston, Oklahoma 73050, USA
[68]University of Oklahoma, Norman, Oklahoma 73019, USA
[69]Oklahoma State University, Stillwater, Oklahoma 74078, USA
[70]Brown University, Providence, Rhode Island 02912, USA
[71]University of Texas, Arlington, Texas 76019, USA
[72]Southern Methodist University, Dallas, Texas 75275, USA
[73]Rice University, Houston, Texas 77005, USA
[74]University of Virginia, Charlottesville, Virginia 22904, USA
[75]University of Washington, Seattle, Washington 98195, USA

(Received 30 August 2012; published 26 October 2012)

We present a measurement of the semileptonic mixing asymmetry for B^0 mesons, $a^d_{\rm sl}$, using two independent decay channels: $B^0 \to \mu^+ D^- X$, with $D^- \to K^+\pi^-\pi^-$; and $B^0 \to \mu^+ D^{*-} X$, with $D^{*-} \to \bar{D}^0\pi^-$, $\bar{D}^0 \to K^+\pi^-$ (and charge conjugate processes). We use a data sample corresponding to 10.4 fb^{-1} of $p\bar{p}$ collisions at $\sqrt{s} = 1.96$ TeV, collected with the D0 experiment at the Fermilab Tevatron collider. We extract the charge asymmetries in these two channels as a function of the visible proper decay length of the B^0 meson, correct for detector-related asymmetries using data-driven methods, and account for dilution from charge-symmetric processes using Monte Carlo simulation. The final measurement combines four signal visible proper decay length regions for each channel, yielding $a^d_{\rm sl} = [0.68 \pm 0.45(\text{stat}) \pm 0.14(\text{syst})]\%$. This is the single most precise measurement of this parameter, with uncertainties smaller than the current world average of B factory measurements.

DOI: 10.1103/PhysRevD.86.072009 PACS numbers: 11.30.Er, 12.15.Ff, 14.40.Nd

I. INTRODUCTION

Fundamental asymmetries in the interactions of elementary particles influence the large-scale behavior of the Universe. Of particular interest is the process of baryogenesis, whereby an initially symmetric system of particles and antiparticles produced by the big bang evolved into the observed matter-dominated universe of the present day. Current theoretical models, building on the work of Sakharov [1], require CP-symmetry violating processes in order for baryogenesis to have occurred in the very early universe [2–5]. As such, studies of asymmetries in particle physics experiments have an influence far beyond the scale that they probe directly.

CP symmetry implies that physical processes are invariant under the combined parity and charge conjugation transformations. The standard model (SM) of particle physics is not CP symmetric as it stands, due to a complex phase in the quark mixing matrix of the weak interaction, which has been measured to be nonzero [6]. While such SM processes introduce some degree of CP violation (CPV), the effects in the quark sector are far too weak to explain the observed matter dominance of the Universe [7]. Consequently, it is important to search for further non-SM sources of CPV.

Studies of neutral B meson oscillations, whereby a neutral meson changes into its own antiparticle via a box-diagram-mediated weak interaction [6], can provide a sensitive probe for such CPV processes. The semileptonic mixing asymmetry, defined as

$$a^q_{\rm sl} = \frac{\Gamma(\bar{B}^0_q \to B^0_q \to \ell^+ X) - \Gamma(B^0_q \to \bar{B}^0_q \to \ell^- X)}{\Gamma(\bar{B}^0_q \to B^0_q \to \ell^+ X) + \Gamma(B^0_q \to \bar{B}^0_q \to \ell^- X)}, \quad (1)$$

*Visitor from Augustana College, Sioux Falls, SD, USA.
†Visitor from The University of Liverpool, Liverpool, United Kingdom.
‡Visitor from UPIITA-IPN, Mexico City, Mexico.
§Visitor from DESY, Hamburg, Germany.
‖Visitor from SLAC, Menlo Park, CA, USA.
¶Visitor from University College London, London, United Kingdom.
**Visitor from Centro de Investigacion en Computacion - IPN, Mexico City, Mexico.
††Visitor from ECFM, Universidad Autonoma de Sinaloa, Culiacán, Mexico.
‡‡Visitor from Universidade Estadual Paulista, São Paulo, Brazil.

allows the effects of any CP-violating processes to be directly observed in terms of the resulting asymmetry of the decay products. Here ℓ denotes a charged lepton of any flavor, and q represents the flavor of the non-b valence quark of the meson.

In the standard model, the semileptonic mixing asymmetry is related to the properties of the corresponding B meson system, namely, the mass difference $\Delta M_q = M(B^0_{qH}) - M(B^0_{qL})$, the decay-width difference $\Delta\Gamma_q = \Gamma(B^0_{qL}) - \Gamma(B^0_{qH})$, and the CP-violating phase ϕ_q, by

$$a^q_{\rm sl} = \frac{|\Gamma^q_{12}|}{|M^q_{12}|}\sin\phi_q = \frac{\Delta\Gamma_q}{\Delta M_q}\tan\phi_q. \quad (2)$$

Here the states B^0_{qH} and B^0_{qL} are the heavy and light mass eigenstates of the B meson system, which differ from the flavor eigenstates. M^q_{12} and Γ^q_{12} are, respectively, the off-diagonal elements of the mass and decay matrices [6].

The standard model predictions [8] for both $a^s_{\rm sl}$ and $a^d_{\rm sl}$ are very small:

$$a^d_{\rm sl} = (-0.041 \pm 0.006)\%, \quad (3)$$

$$a^s_{\rm sl} = (0.0019 \pm 0.0003)\%. \quad (4)$$

These predictions are effectively negligible compared to the current experimental precision. Hence, the measurement of any significant deviation from zero is an unambiguous signal of new physics, which could lead to order-of-magnitude enhancements of $|a^d_{\rm sl}|$ [9].

The B^0 semileptonic mixing asymmetry, $a^d_{\rm sl}$, has been extensively studied by the B factories operating at the $\Upsilon(4S)$ resonance, including measurements by the CLEO [10,11], *BABAR* [12,13], and Belle [14] Collaborations. The current world average of these measurements is [6]

$$a^d_{\rm sl} = (-0.05 \pm 0.56)\%. \quad (5)$$

Additional inclusive measurements from LEP [15–17] and D0 [18] are subject to contamination from B^0_s mesons, and the extraction of $a^d_{\rm sl}$ relies upon assumptions about the contribution from $a^s_{\rm sl}$.

The recent evidence for a nonzero dimuon charge asymmetry by the D0 experiment is sensitive to the linear combination of B^0 and B^0_s mixing asymmetries, with approximately equal contributions from each source [19]. The measurement constrains a band in the $(a^d_{\rm sl}, a^s_{\rm sl})$ plane, which is inconsistent with the SM prediction at the 3.9 standard deviation level. By dividing the sample into two components with different relative contributions from B^0 and B^0_s, the semileptonic asymmetries are measured to be

$$a^d_{\rm sl}(\mu\mu) = (-0.12 \pm 0.52)\%, \quad (6)$$

$$a^s_{\rm sl}(\mu\mu) = (-1.81 \pm 1.06)\%, \quad (7)$$

where the measurements have a correlation coefficient of -0.799. The above extraction assumes that any new source of CPV entering the dimuon asymmetry does so through B mixing. Alternative hypotheses, for example, new sources of dimuons from non-SM processes, cannot be excluded.

Recent searches for CPV in $B^0_s \to J/\psi\phi$ decays from the D0 [20], CDF [21], and LHCb [22] Collaborations find agreement of the CP-violating phase ϕ_s with SM predictions. Given the current body of experimental evidence, improved measurements of both $a^d_{\rm sl}$ and $a^s_{\rm sl}$ are required in order to constrain the possible sources of new physics in B meson mixing and decay [23].

This article describes the measurement of the semileptonic mixing asymmetry for B^0_d mesons,

$$a^d_{\rm sl} = \frac{\Gamma(\bar{B}^0 \to B^0 \to \ell^+ D^{(*)-} X) - \Gamma(B^0 \to \bar{B}^0 \to \ell^- D^{(*)+} X)}{\Gamma(\bar{B}^0 \to B^0 \to \ell^+ D^{(*)-} X) + \Gamma(B^0 \to \bar{B}^0 \to \ell^- D^{(*)+} X)}, \quad (8)$$

without the use of initial-state flavor tagging. The flavor of the B^0 meson at the time of decay is determined by the charge of the muon in the semileptonic decay. Two separate decay channels are used:

(1) $B^0 \to \mu^+ \nu D^- X$, with $D^- \to K^+\pi^-\pi^-$ (plus charge conjugate process);
(2) $B^0 \to \mu^+ \nu D^{*-} X$, with $D^{*-} \to \bar{D}^0\pi^-$, $\bar{D}^0 \to K^+\pi^-$ (plus charge conjugate process).

The two channels are treated separately, with each being used to extract $a^d_{\rm sl}$ before the final measurements are combined. For clarity, the two channels are, respectively, denoted by μD and μD^* throughout this paper, with the appropriate combinations of charges implied. Charges are only explicitly shown when required to describe the asymmetry measurement, or to avoid possible ambiguity.

II. ANALYSIS OVERVIEW

Experimentally, the semileptonic mixing asymmetry is expressed as

$$a^d_{\rm sl} = \frac{A - A_{\rm BG}}{F^{\rm osc}_{B^0}}. \quad (9)$$

Here, A is the measured raw asymmetry, defined by

$$A = \frac{N_{\mu^+ D^{(*)-}} - N_{\mu^- D^{(*)+}}}{N_{\mu^+ D^{(*)-}} + N_{\mu^- D^{(*)+}}} \equiv \frac{N_{\rm diff}}{N_{\rm sum}}, \quad (10)$$

where $N_{\mu^\pm D^{(*)\mp}}$ is the number of reconstructed $\mu^\pm D^{(*)\mp}$ signal candidates. The sum is extracted by fitting the total mass distribution, and the difference by fitting the difference of two charge-specific mass distributions. The term $A_{\rm BG}$ accounts for inherent detector-related background (BG) asymmetries, for example, due to the different reconstruction efficiencies for positively and negatively charged kaons. The denominator $F^{\rm osc}_{B^0}$ is defined as the fraction of all $\mu D^{(*)}$ signal events that arise from decays of B^0 mesons after they have oscillated. It is required to account for $D^{(*)}$ mesons arising from direct B^0 decays,

decays of $B^{\pm}$ and B_s^0 mesons, or direct hadronization from $c\bar{c}$ quarks. All background asymmetries are extracted using data-driven methods, while Monte Carlo (MC) simulation is used to determine the fraction of B^0 mesons that have undergone mixing prior to decay.

This measurement assumes that the initial production of B^0-$\bar{B}^0$ is symmetric, and that there is no asymmetry in the decays of unmixed B^0 or $\bar{B}^0$ mesons (that would imply CPT violation), and no direct CP asymmetry in the semileptonic decays to charm states, or the decay of these charm states to the indicated products. With these assumptions, any observed semileptonic asymmetry would have to arise due to the mixing process.

The B^0 meson has a mixing frequency $\Delta M_d = 0.507 \pm 0.004\ \text{ps}^{-1}$, of comparable scale to the lifetime $\tau(B^0) = 1.518 \pm 0.007$ ps [6]. Hence the fraction of oscillated B^0 mesons is a strong function of the measured decay time. The proper decay length ct for a particle is given by

$$ct = \frac{L}{\beta\gamma} = L \cdot \frac{cM}{p} = L_{xy} \cdot \frac{cM}{p_T}, \tag{11}$$

where γ and β are the usual relativistic kinematic quantities; p, M and L are, respectively, the particle momentum, mass and decay length in the detector reference frame. The best precision is obtained by using the transverse quantities L_{xy} and p_T, due to finer instrumentation for tracking in this plane. The transverse decay length L_{xy} is the projection of the vector pointing from the production to the decay vertex of the B meson onto the B meson transverse momentum direction. It can be negative due to the limited spatial resolution of the detector.

For semileptonic decays, the missing energy due to the undetected neutrino results in the measured transverse momentum being underestimated with respect to the actual value. Hence the measured variable is actually the visible proper decay length (VPDL):

$$\text{VPDL}\,(B) = L_{xy}(B) \cdot \frac{cM(B)}{p_T(\mu D)}. \tag{12}$$

The dilution $F^{\text{osc}}_{B^0}$ is a very strong function of this variable, increasing monotonically with VPDL. To exploit this behavior, the measurements of all asymmetries are performed separately in bins of VPDL(B^0). These measurements are then combined for each channel to obtain the final measurement. The selected VPDL(B^0) bins are defined by the edges $\{-0.10, 0.00, 0.02, 0.05, 0.10, 0.20, 0.60\}$ cm. The $\mu D^{(*)}$ signal contributions outside of this range are found to be negligible. The first two bins in VPDL have negligible contributions from oscillated B^0 mesons, and are not included in the final a^d_{sl} measurement. They represent a control region in which the measured raw asymmetry should be dominated by the background contribution, i.e., $A - A_{\text{BG}} \approx 0$.

There can be significant ($\sim 1\%$) asymmetries due to detector effects. In particular, the material and detector elements that a particle traverses are different for positively and negatively charged particles, as a result of the specific orientation of magnetic fields in the central tracking and muon detectors. In this analysis, such effects are removed to first order by reweighting all events, such that the total weight of events collected in each of the four (solenoid, toroid) magnet polarity configurations is the same (see Sec. III). Remaining asymmetries are of order 0.1%, and are corrected using data-driven methods.

To avoid possible experimental bias, the central values of the raw asymmetries were hidden until all analysis methods were finalized. Initially this was achieved by randomly assigning all candidate charges; later, to allow the background asymmetries to be examined, the true charges were used, but unknown offsets were added to the raw charge asymmetries.

The D0 detector is briefly described in Sec. III, highlighting those features most relevant for this measurement. The event selection and raw asymmetry extraction are described in Secs. IV, V, and VI. The determination of background asymmetries is described in Sec. VII, while Sec. VIII covers the extraction of the oscillated B^0 fraction. The results and conclusions are presented in Secs. IX, X, XI, and XII.

III. THE D0 DETECTOR

The D0 detector has been described in detail elsewhere [24]. The most important detector components for this measurement are the central tracking system, the muon detectors, and the magnets.

The central tracking system comprises a silicon microstrip tracker (SMT) and a central fiber tracker (CFT), both located within a 2 T superconducting solenoidal magnet. The SMT has $\approx 800\,000$ individual strips, with typical pitch of 50–80 μm, and a design optimized for tracking and vertexing capability at pseudorapidities of $|\eta| < 2.5$, where $\eta = -\ln[\tan(\theta/2)]$ and θ is the polar angle with respect to the beam axis. The system has a six-barrel longitudinal structure, each with a set of four layers arranged axially around the beam pipe, and interspersed with 16 radial disks. In the spring of 2006, a "Layer 0" barrel detector with 12 288 additional strips was installed [25], and two radial disks were removed. This upgrade defines the chronological boundary between the two running periods, denoted Run IIa and Run IIb. The sensors of Layer 0 are located at a radius of 17 mm from the colliding beams. The CFT has eight thin coaxial barrels, each supporting two doublets of overlapping scintillating fibers of 0.835-mm diameter, one doublet being parallel to the collision axis, and the other alternating by $\pm 3°$ relative to the axis. Light signals are transferred via clear fibers to solid-state photon counters that have $\approx 80\%$ quantum efficiency.

A muon system resides beyond the calorimeter, and consists of a layer of tracking detectors and scintillation trigger counters before a 1.8-T toroidal magnet, followed by two similar layers after the toroid. Tracking at $|\eta| < 1$ relies on 10-cm wide drift tubes, while 1-cm minidrift tubes are used at $1 < |\eta| < 2$.

The polarities of both the solenoidal and toroidal magnets were regularly reversed during data acquisition, approximately every two weeks, resulting in almost equal beam exposure in each of the four polarity configurations. This feature of the D0 detector is crucial in reducing detector-related asymmetries, for example, due to the different trajectories of positive and negative muons as they traverse the magnetic fields in the detector.

IV. EVENT SELECTION

This analysis uses data collected by the D0 detector from 2002 to 2011, corresponding to approximately 10.4 fb^{-1} of integrated luminosity, and representing the full Tevatron Run II sample of $p\bar{p}$ collisions at center-of-mass energy $\sqrt{s} = 1.96$ TeV. Signal candidates are collected using single and dimuon triggers, which may also impose additional criteria. To avoid lifetime-dependent trigger efficiencies, which are difficult to model in simulation, events that exclusively satisfy muon triggers with track impact-parameter requirements are removed.

For both channels, events are considered for selection if they contain a muon candidate with reconstructed track segments both inside and outside the toroid magnet. The muon candidate must be matched to a track in the central tracking system, with at least three hits in both the SMT and CFT. In addition, it must have transverse momentum $p_T > 2$ GeV/c, and total momentum $p > 3$ GeV/c.

For events fulfilling these requirements, $D^{(*)\mp}$ candidates are constructed by combining three other tracks associated with the same initial $p\bar{p}$ interaction. Each track must satisfy $p_T > 0.7$ GeV/c, and have at least two hits in both the SMT and CFT. The tracks must have a summed charge of magnitude $|q| = 1$, with an opposite sign to the muon charge. Each of the tracks comprising the like-charge pair is assigned the charged pion mass [6]. The third track, which has the same charge as the muon, is assigned the charged kaon mass [6].

A. μD channel

For the $D^- \to K^+\pi^-\pi^-$ decay (and charge conjugate process), the three hadron tracks must be consistent with originating at a single common vertex, with a vertex fit to the three tracks satisfying $\chi^2(\text{vertex}) < 16$. These tracks are combined to construct a D^- candidate. The resulting D^- trajectory must be consistent with forming a common vertex with the muon to reconstruct a B^0 candidate. The cosine of the angle θ_T^D between the momentum and trajectory vectors of the D^- meson in the transverse plane must satisfy $\cos(\theta_T^D) > 0.0$; i.e., the two vectors must point to the same hemisphere. The invariant masses must satisfy $1.6 < M(D^-) < 2.1$ GeV/c^2 and $2.0 < M(B^0) < 5.5$ GeV/c^2.

At this preselection stage, a total of $\sim 8.3 \times 10^8$ candidates remain, dominated by random three-track combinations incorrectly associated with a real muon. A fit to the $M(K\pi\pi)$ distribution yields $1\,629\,000 \pm 29\,000\,\mu D$ combinations. To increase the signal fraction of the sample, a log likelihood ratio (LLR) method is utilized [26] to construct a single discriminating parameter from the combination of 13 individual variables: the D^- transverse decay length $L_{xy}(D^-)$ and its significance $L_{xy}(D^-)/\sigma[L_{xy}(D^-)]$; the track isolation I of the kaon, the leading pion, and the trailing pion; the transverse momentum of the kaon, the leading pion, and the trailing pion; the invariant mass of the reconstructed B^0 candidate, $M(\mu D)$; the χ^2 of the vertex fit for both the $K\pi\pi$ and μD vertices; and the two-dimensional angular separation ΔR of the kaon and trailing pion, and of the two pions. The two-dimensional angular separation of two tracks is defined as $\Delta R = \sqrt{\Delta\phi^2 + \Delta\eta^2}$, where η is the pseudorapidity and ϕ is the azimuthal angle of each track. The track isolation I is the momentum of a particle divided by the sum of momenta of all tracks contained in a cone of size $\Delta R = 0.5$ around the particle. Tracks corresponding to the other three final state particles for this candidate are excluded from the sum.

The signal distributions required to construct the LLR discriminant are obtained from MC simulated events, in which the signal channel is required at generation, and the reconstructed tracks are required to match the correct particles at the generator level. For all MC studies described in this article, events are generated using PYTHIA version 6.409 [27], interfaced with EVTGEN [28] to model the decays of particles containing b and c quarks. Generated events are processed by a GEANT based detector simulation, and overlaid with data from randomly collected bunch crossings to simulate pileup from multiple interactions. The MC samples are then reconstructed using the same software as used for data. The corresponding background distributions are obtained from sideband events in real data, defined by $[1.660 < M(K\pi\pi) < 1.760, 1.964 < M(K\pi\pi) < 2.064]\,\text{GeV}/c^2$, with each sideband scaled to give equal weight to the final distributions.

Candidates enter the final data sample if the LLR discriminant exceeds a value L_{min}, chosen to maximize the signal significance in data, $N_S/\sqrt{N_S + N_B}$, where N_S and N_B are the number of μD signal and background events, respectively. This figure of merit is found to correspond to the minimum uncertainty on the measured raw asymmetry. The optimal requirement is determined separately in each VPDL bin, and the value of L_{min} decreases for longer lifetimes, where the background from random track combinations is significantly reduced.

After applying all selection requirements, the total μD signal yield is $\sim$740 000, with an overall efficiency of approximately 44% with respect to the preselection sample. The signal efficiency in VPDL bins 3–6, used to extract a_{sl}^d, ranges from 53% to 72%. The $M(K\pi\pi)$ invariant mass distribution over the full VPDL range is shown in Fig. 1.

B. μD^* channel

For the $D^{*-} \to \bar{D}^0\pi^-$, $\bar{D}^0 \to K^+\pi^-$ decay (and charge conjugate process), D^0 candidates are reconstructed by

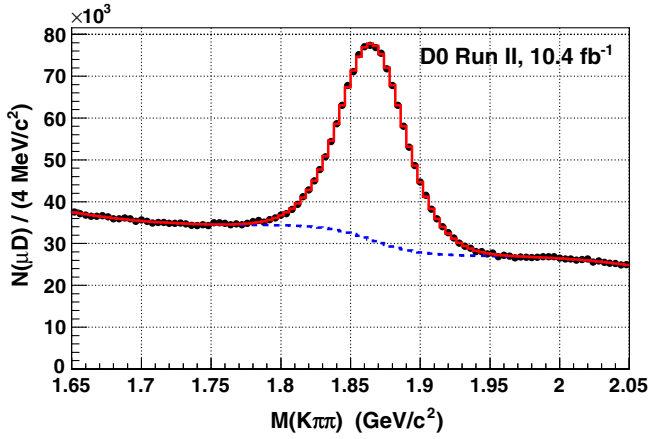

FIG. 1 (color online). Distribution of the invariant mass $M(K\pi\pi)$ after all selections have been applied, for the μD channel. The events have been weighted using the method described in Sec. V. The histogram shows the fit model used to extract the yield, with the background component drawn separately as a dashed line (see Sec. VI for fit models).

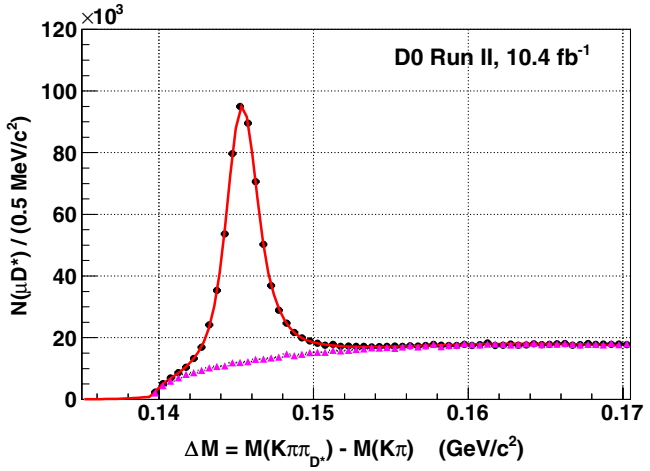

FIG. 2 (color online). Distribution of the invariant mass difference $\Delta M \equiv [M(K\pi\pi_{D^*}) - M(K\pi)]$, for the μD^* channel. The events have been weighted using the method described in Sec. V. The solid line shows the fit model used to extract the yield. The triangular data points show the corresponding distribution for μD^* candidates in which the three hadrons have the same charge, scaled to give the same yield as the signal sample, in the sideband region $0.155 < \Delta M < 0.170$ GeV/c^2 (see Sec. VI for fit models).

combining a pair of oppositely charged tracks passing the criteria described above. The two tracks must form a common secondary vertex, and are used to reconstruct the parent $\bar{D}^0$ candidate, which must satisfy $p_T(\bar{D}^0) > 0.7$ GeV/c and $|\eta(\bar{D}^0)| < 2.0$. The invariant mass must lie in the range $1.7 < M(K\pi) < 2.0$ GeV/c^2.

Next, an additional track is combined with the $\bar{D}^0$ candidate, which must have the opposite charge to the muon, and be consistent with forming a common vertex with the $\bar{D}^0$. This track is allocated the mass of the charged pion, and is here denoted π_{D^*}. The difference in the invariant masses of the D^{*-} and $\bar{D}^0$ candidates must satisfy $0.120 < [\Delta M \equiv M(K\pi\pi_{D^*}) - M(K\pi)] < 0.200$ GeV/c^2. In addition, the displacement of the $\bar{D}^0 \to K^+\pi^-$ decay vertex with respect to the $D^{*-} \to \bar{D}^0\pi^-$ decay vertex must correspond to a significance of at least 3σ, i.e.,

$$S \equiv \sqrt{(\epsilon_T/\sigma_T)^2 + (\epsilon_L/\sigma_L)^2} > 3, \tag{13}$$

where $\epsilon_{T(L)}$ and $\sigma_{T(L)}$ represent the distance and corresponding uncertainty of the transverse (longitudinal) displacement between the two vertices.

The D^{*-} candidate is then combined with the muon, to form a B^0 candidate. The muon, $\bar{D}^0$, and π_{D^*} trajectories must be consistent with arising from a common vertex, and the invariant mass of the B^0 must satisfy $2.0 < M(\mu D^*) < 5.5$ GeV/c^2.

The final event selection requirement utilizes a boosted decision tree to further suppress backgrounds [29]. A total of 22 variables are selected as inputs:

(i) transverse momentum $p_T(K)$, $p_T(\pi)$, $p_T(\pi_{D^*})$, $p_T(\bar{D}^0)$;
(ii) isolation $I(K)$, $I(\pi)$, $I(\pi_{D^*})$, $I(D^*)$, $I(B^0)$;
(iii) angular separation $\Delta R(K, \pi)$, $\Delta R(K, \pi_{D^*})$, $\Delta R(\pi, \pi_{D^*})$, $\Delta R(\bar{D}^0, \mu)$;
(iv) transverse decay length $L_{xy}(\bar{D}^0)$, error $\sigma[L_{xy}(\bar{D}^0)]$, and significance $L_{xy}(\bar{D}^0)/\sigma[L_{xy}(\bar{D}^0)]$;
(v) cosine of the angle, in the transverse plane, between the $\bar{D}^0$ momentum vector and the position vector of the $\bar{D}^0$ decay vertex with respect to (a) the primary $p\bar{p}$ interaction vertex and (b) the B^0 decay vertex;
(vi) cosine of the angle, in the transverse plane, between the D^* momentum vector and the position vector of the D^* decay vertex with respect to the primary vertex;
(vii) decay vertex fit quality $\chi^2(B^0)$; and
(viii) invariant mass $M(K\pi)$ and $M(\mu D^*)$.

The signal distributions are taken from MC simulation, in which the signal channel is generated exclusively by forcing the required decays in EVTGEN, and the reconstructed tracks are required to match the correct particles at the generator level. The background distributions are taken from real data, in which the kaon and two pions all have the same charge, and the muon has the opposite charge. The choice of the boosted decision tree cut used to define the final data sample is made separately for Run IIa and Run IIb samples, and for each VPDL(B^0) region, to optimize the signal significance in each case.

After application of all selection criteria, the sample contains ~545 000 μD^* signal candidates. The ΔM distribution for the full VPDL range is shown in Fig. 2.

V. EVENT WEIGHTS

In any given configuration of the solenoidal and toroidal magnet polarities, there can be detector-related asymmetries. These originate from differing detection efficiencies

for positively and negatively charged particles, in turn caused by their different trajectories as they bend through the magnetic fields in the detector. The regular reversal of both magnet polarities suppresses such effects. To ensure maximal cancellation of these instrumental asymmetries, an additional event-by-event weighting is applied such that the sums of weights in each (solenoid, toroid) configuration are the same, for a given sample.

The weights are determined after applying the final event selections, by counting the total number of events in each of the four solenoid and toroid magnet polarity configurations. The weight for an event collected in a polarity configuration $i = \{1, 2, 3, 4\}$ is defined as $N_{\rm min}/N_i$ where N_i is the number of events in this polarity configuration, and $N_{\rm min}$ is the smallest of the four yields $N_{1,2,3,4}$. This procedure is performed separately for each channel, and for each VPDL(B^0) bin. Event weights are typically in the range 0.90–1.00, with very little variation between VPDL bins. For the unbinned samples, the total signal yields after event weighting are $N(\mu D) = 721\,519 \pm 3537$, and $N(\mu D^*) = 519\,066 \pm 3446$, as shown in Figs. 1 and 2.

VI. EXTRACTING THE RAW ASYMMETRY

The raw asymmetry is extracted by fitting the invariant mass distributions $M(K\pi\pi)$ (or ΔM) for the $D^{(*)}$ candidates. The sum distribution $H_{\rm sum}$ is constructed by weighting all $\mu D^{(*)}$ candidates according to the magnet polarity weight. A difference distribution $H_{\rm diff}$ is constructed by taking the difference between the $\mu^+ D^{(*)-}$ and $\mu^- D^{(*)+}$ distributions. The sum and difference distributions are modeled by, respectively, the functions:

$$F_{\rm sum} = F^{\rm BG}_{\rm sum} + N_{\rm sum} \cdot F^{\rm sig}, \tag{14}$$

$$F_{\rm diff} = F^{\rm BG}_{\rm diff} + A \cdot N_{\rm sum} \cdot F^{\rm sig}, \tag{15}$$

where $N_{\rm sum}$ is the total $\mu D^{(*)}$ yield, and A is the corresponding raw charge asymmetry defined in Eq. (10). Different models are used to parametrize the backgrounds for the sum ($F^{\rm BG}_{\rm sum}$) and difference ($F^{\rm BG}_{\rm diff}$) histograms, while a single model $F^{\rm sig}$ is used for the signal in both cases. The yields, asymmetries, and signal and background parameters in these models are extracted by a simultaneous binned fit to the two distributions, to minimize the total χ^2 with respect to the fitting functions.

A. μD channel

The physical width of the D^- meson is negligible compared to the detector resolution; therefore, the signal parametrization is chosen based on studies of simulated data to determine the mass resolution for this channel. The signal is modeled by the sum of two Gaussian functions constrained to have the same mean, but with different widths and relative normalizations:

$$F^{\rm sig}(D) = \frac{1}{\sqrt{2\pi}}\Big[f_{G1} \cdot \frac{1}{\sigma_1} \cdot e^{-(x-M_D)^2/(2\sigma_1^2)} + (1 - f_{G1}) \cdot \frac{1}{\sigma_2} \cdot e^{-(x-M_D)^2/(2\sigma_2^2)}\Big], \tag{16}$$

where x is the reconstructed invariant mass of the D^- candidate, M_D is the mean of the Gaussian peak, $\sigma_{1,2}$ are the widths of the first and second Gaussians, and f_{G1} is the fraction of the signal in the first Gaussian peak.

The background in the sum distribution exhibits slightly different behavior for each VPDL bin, hence a flexible parametrization is selected to provide good agreement in all bins, comprising the sum of three possible components: a low-order polynomial function, a falling exponential function, and a hyperbolic tangent function:

$$F^{\rm BG}_{\rm sum}(D) = (N_{\rm tot} - N_{\rm sum}) \cdot \{f_{\rm tanh} \cdot F_{\rm tanh} + (1 - f_{\rm tanh}) \cdot f_{\rm poly} \cdot F_{\rm poly} + (1 - f_{\rm tanh}) \cdot (1 - f_{\rm poly}) \cdot F_{\rm exp}\}. \tag{17}$$

Here $f_{\rm tanh}$ and $f_{\rm poly}$ are free parameters between zero and one, controlling the relative contributions of the three components.

The polynomial function includes a constant, linear, and cubic term:

$$F_{\rm poly} = C_1 + p_1 \cdot (x - x_{\rm mid}) + p_3 \cdot (x - x_{\rm mid})^3, \tag{18}$$

where p_1 and p_3 are free parameters of the fit, and $x_{\rm mid}$ is the midpoint of the fitting range. The exponential term is

$$F_{\rm exp} = C_2 \cdot e^{r(x - x_{\rm min})}, \tag{19}$$

where r is a free parameter and $x_{\rm min}$ is the lower limit of the fitting range.

Finally, a hyperbolic tangent function described by

$$F_{\rm tanh} = C_3 \cdot [1 - \tanh(k \cdot (x - M_D))] \tag{20}$$

is used to model the effects of partially reconstructed decays, and reflections from decays into other three-track combinations. Monte Carlo simulations confirm that this parametrization is a good model for this source of background, which includes contributions from D^- decays to $K^+\pi^-\pi^-\pi^0$, $\pi^+\pi^-\pi^-\pi^0$, and $K^+K^-\pi^-$; $\bar{D}^0$ decays to four charged hadrons; and decays of $D^{*-} \to \bar{D}^0\pi^-$ with $\bar{D}^0 \to K^+\pi^-\pi^0$, where the π^0 is not reconstructed. The steepness of the threshold, denoted by k in Eq. (20), is controlled by the detector mass resolution. As such it is fixed according to the widths of the two Gaussian peaks:

$$k = \frac{1}{\sqrt{2\sigma^2_{\rm mean}}}, \tag{21}$$

where $\sigma_{\rm mean} = f_{G1} \cdot \sigma_1 + (1 - f_{G1}) \cdot \sigma_2$ is the weighted mean of the two widths.

All three individual components are normalized to have a unit area in the fitting range, by suitable choice of the

constants C_1, C_2, and C_3. The overall normalization is set by subtracting the fitted number of signal events ($N_{\rm sum}$) from the total event count in the sample ($N_{\rm tot}$). Using the total event count as a constraint in this way improves the fit precision. The free parameters are the two fractions, $f_{\rm tanh}$ and $f_{\rm poly}$, the two polynomial coefficients, $p_{1,3}$, and the argument of the exponential function, r. This empirical choice provides good agreement with the data, with relatively few free parameters, over a range of different background shapes. To improve fit precision and stability, each term in $F^{\rm BG}_{\rm sum}$ is only used if it improves the fit probability. As a result, for VPDL bins 1–3 the exponential component is removed; for bin 6, the cubic term is removed.

For the difference fit, the overall normalization $N^{\rm BG}_{\rm diff}$ of the background is fixed according to the observed number of D^+ and D^- events, and the signal contribution:

$$N^{\rm BG}_{\rm diff} = N^{+}_{\rm tot} - N^{-}_{\rm tot} - A \cdot N_{\rm sum}, \tag{22}$$

where $N^{\pm}_{\rm tot}$ is the sum of all event weights for $D^{\pm}$ candidates. The background model comprises the same three components as used in the fit to the sum. The threshold component is modeled by the same shape as in the sum fit, with the yield scaled by a free parameter ($a_{\rm tanh}$) accounting for the possible charge asymmetry from this contribution. The combinatorial background is modeled by the sum of exponential and polynomial terms, with the shape parameters common to the sum fit, and the yield constrained by Eq. (22) after the contribution of the threshold component has been accounted for:

$$\begin{aligned} F^{\rm BG}_{\rm diff}(D) = N^{\rm BG}_{\rm diff} \cdot \{ & a_{\rm tanh} \cdot f_{\rm tanh} \cdot F_{\rm tanh} \\ & + (1 - a_{\rm tanh} \cdot f_{\rm tanh}) \cdot f_{\rm poly} \cdot F_{\rm poly} \\ & + (1 - a_{\rm tanh} \cdot f_{\rm tanh}) \cdot (1 - f_{\rm poly}) \cdot F_{\rm exp} \}. \end{aligned} \tag{23}$$

This function has only one additional free parameter, with respect to the fit over the sum of all candidates, namely, the asymmetry on the hyperbolic tangent, $a_{\rm tanh}$. The corresponding asymmetry term for the polynomial component is eliminated by applying the constraint from Eq. (22).

In total, there are 12 free parameters in the mass fit for this channel, six describing the signal, and six describing the background. The default fit is performed over the range $[1.65 < M(K\pi\pi) < 2.05]$ GeV/c^2, using 100 bins of width 4 MeV/c^2, with variations on both the fitting range and the bin width considered as sources of systematic uncertainty.

B. μD^* channel

For this channel the invariant mass difference distribution $\Delta M = M(K\pi\pi_{D^*}) - M(K\pi)$ is fitted to extract the raw asymmetry. The proximity to the pion production threshold at approximately 140 MeV/c^2 leads to phase-space effects that tend to distort the signal and background distributions. To account for these effects, and based on studies of MC simulation data, the signal is modeled by a skewed triple-Gaussian function, i.e., three Gaussian peaks constrained to have the same mean, but with different widths and relative contributions, and each multiplied by a threshold shape:

$$\begin{aligned} F^{\rm sig}(D^*) = & f_{G1} \cdot G_{\rm sk}(x, \sigma_1, M, s) \\ & + (1 - f_{G1}) \cdot f_{G2} \cdot G_{\rm sk}(x, \sigma_2, M, s) \\ & + (1 - f_{G1}) \cdot (1 - f_{G2}) \cdot G_{\rm sk}(x, \sigma_3, M, s), \end{aligned} \tag{24}$$

where $G_{\rm sk}$ is the skewed Gaussian function:

$$G_{\rm sk}(x, \sigma_i, M, s) = \frac{1}{\sqrt{2\pi}\sigma_i} \cdot E\left[-s \frac{(x - M)}{\sqrt{2}\sigma_i} \right] \cdot e^{-\frac{(x-M)^2}{2\sigma_i^2}}. \tag{25}$$

Here x is the reconstructed value of ΔM for this D^{*-} candidate, M is the mean of the Gaussian peak, $\sigma_{1,2,3}$ are the widths of the three Gaussians, and $f_{G1,2}$ describe their relative fractional contributions. The function $E(s \cdot y)$ is a threshold shape modeled by the complementary error function, taking the skew s as an input parameter, and defined as

$$E(s \cdot y) = \frac{2}{\sqrt{\pi}} \int_{s \cdot y}^{\infty} e^{-t^2} dt. \tag{26}$$

The background in the sum fit is modeled by the product of a linear function and a power law function with a threshold at the charged pion mass M_π [6], and three free parameters a, b, and d:

$$F^{\rm BG}_{\rm sum}(D^*) = d \cdot (x - M_\pi)^a \cdot (1 + bx). \tag{27}$$

The background in the difference distribution is modeled by the same shape as used for the sum, but with a different overall scale, quantified by a background asymmetry parameter $a_{\rm BG}$:

$$F^{\rm BG}_{\rm diff}(D^*) = d \cdot a_{\rm BG} \cdot (x - M_\pi)^a \cdot (1 + bx). \tag{28}$$

In total there are 13 free parameters in the fit, nine for the signal, and four describing the background. The default fit is performed over the range $[0.139 < \Delta M < 0.170]$ GeV/c^2, using 62 bins of width 0.5 MeV/c^2, with variations on both the fitting range and the bin width considered as sources of systematic uncertainty.

C. Results

The values of all physics parameters returned by the fits, for both channels, and for each of the six VPDL(B^0) bins are collected in Tables I and II, with examples of the fit projections shown in Fig. 3. Significant positive asymmetries are observed for all VPDL bins, including those in the control region VPDL(B^0) < 0.02 cm. This is expected as a consequence of the positive kaon reconstruction asymmetry, which is described and corrected for in Sec. VII. The two channels have similar statistical precision on the raw

TABLE I. Results of the raw asymmetry fits for the μD channel, in each of the six bins of VPDL(B^0). The uncertainties are statistical, as returned by the fits.

	Bin 1	Bin 2	Bin 3	Bin 4	Bin 5	Bin 6
VPDL(B^0) (cm)	−0.10–0.00	0.00–0.02	0.02–0.05	0.05–0.10	0.10–0.20	0.20–0.60
$N(\mu D)$	42707 ± 1374	155 322 ± 1011	198 874 ± 1105	182 921 ± 1598	113 965 ± 1329	26 939 ± 458
A (%)	2.70 ± 1.28	1.02 ± 0.35	1.16 ± 0.32	1.50 ± 0.33	1.48 ± 0.41	1.20 ± 0.88
$M(D)$ (MeV/c^2)	1866.3 ± 0.6	1865.8 ± 0.2	1865.7 ± 0.2	1865.9 ± 0.2	1865.4 ± 0.2	1864.3 ± 0.3
σ_{G1} (MeV/c^2)	21.6 ± 1.6	19.0 ± 0.9	18.6 ± 1.0	18.3 ± 1.0	18.0 ± 1.7	15.0 ± 3.0
σ_{G2} (MeV/c^2)	39.6 ± 8.8	32.5 ± 1.4	30.1 ± 1.1	29.6 ± 1.3	28.6 ± 1.8	27.0 ± 1.5
f_{G1}	0.67 ± 0.16	0.417 ± 0.071	0.361 ± 0.076	0.363 ± 0.084	0.33 ± 0.13	0.16 ± 0.11
$a_{\tanh}$ (%)	3.75 ± 2.86	1.32 ± 1.04	−0.02 ± 0.84	−0.04 ± 0.79	−0.24 ± 1.00	−0.99 ± 3.66
χ^2/ndf	172/190	199/190	218/190	199/188	213/188	170/189
χ^2(sum)/ndf	81/92	105/92	114/92	108/90	123/90	79/91
χ^2(diff)/ndf	91/98	94/98	104/98	92/98	90/98	91/98

asymmetries, except for the first VPDL bin, where the sensitivity of the μD channel is significantly reduced by the increased background from random three-track combinations close to the primary $p\bar{p}$ interaction. The μD^* channel is less susceptible to such effects, due to the intermediate resonance in the decay.

The raw asymmetry measurement method is validated by the use of ensemble tests, in which the fits to data are repeated several thousand times with the $\mu^{\pm} D^{(*)\mp}$ charges randomized independently for each fit. Different input asymmetries are simulated, ranging from −5% to +5%, and the distribution of asymmetries extracted from the fits are examined. For all cases, the distributions are well modeled by Gaussian peaks, with a central value consistent with the input asymmetry, and a width consistent with the corresponding uncertainty reported in Tables I and II. A similar approach is used to confirm that the optimal precision is obtained by maximizing the signal significance.

D. Systematic uncertainties

Several variations of the fits are performed to extract the raw asymmetry from the data, in order to examine the resulting spread of measured values, and assign an appropriate systematic uncertainty. These variations are considered for all cases where there is a reasonable alternative to the choices made for the nominal fit, namely,

(i) the lower and upper limits of the fitting region are varied to a number of different options within a 50 MeV/c^2 (10 MeV/c^2) range of the nominal choice for the $\mu D^{(*)}$ case;

(ii) the bin width is varied, with alternative widths of 2–20 MeV/c^2 for the μD case, and 0.5–2.0 MeV/c^2 for the μD^* case;

(iii) for the μD channel, the function $F_{\text{sum}}^{\text{BG}}$ used to model the background of the sum distribution is changed to three alternative models in addition to the nominal choice; in one alternative, the polynomial is fixed to a linear function; in another, the

TABLE II. Results of the raw asymmetry fits for the μD channel, in each of the six bins of VPDL(B^0). The uncertainties are statistical, as returned by the fits.

	Bin 1	Bin 2	Bin 3	Bin 4	Bin 5	Bin 6
VPDL(B^0) (cm)	−0.10–0.00	0.00–0.02	0.02–0.05	0.05–0.10	0.10–0.20	0.20–0.60
$N(\mu D^*)$	59 823 ± 2398	151 585 ± 1677	132 227 ± 1092	104 463 ± 921	58 409 ± 651	12 029 ± 233
A (%)	1.82 ± 0.67	1.10 ± 0.30	0.94 ± 0.30	1.38 ± 0.33	2.11 ± 0.44	0.55 ± 0.99
M (MeV/c^2)	145.08 ± 0.06	145.07 ± 0.02	145.03 ± 0.02	144.99 ± 0.02	144.97 ± 0.03	145.00 ± 0.06
σ_{G1} (MeV/c^2)	0.76 ± 0.11	1.59 ± 0.12	1.72 ± 0.09	1.75 ± 0.12	1.67 ± 0.15	1.39 ± 0.23
σ_{G2} (MeV/c^2)	1.45 ± 0.30	0.84 ± 0.03	0.86 ± 0.02	0.90 ± 0.03	0.90 ± 0.04	0.79 ± 0.11
σ_{G3} (MeV/c^2)	3.78 ± 0.76	3.45 ± 0.30	3.89 ± 0.31	3.87 ± 0.32	3.74 ± 0.30	2.92 ± 0.36
f_{G1}	0.32 ± 0.14	0.39 ± 0.03	0.41 ± 0.02	0.38 ± 0.02	0.38 ± 0.04	0.44 ± 0.10
f_{G2}	0.64 ± 0.05	0.69 ± 0.05	0.74 ± 0.04	0.74 ± 0.04	0.69 ± 0.06	0.52 ± 0.17
s	0.368 ± 0.083	0.470 ± 0.032	0.510 ± 0.024	0.541 ± 0.025	0.574 ± 0.037	0.508 ± 0.079
a_{BG} (%)	1.25 ± 0.16	1.17 ± 0.22	−0.10 ± 0.39	−0.19 ± 0.53	0.18 ± 0.77	−0.94 ± 1.41
χ^2/ndf	133/113	138/113	203/107	153/107	165/107	150/107
χ^2(sum)/ndf	80/53	84/53	159/53	94/53	94/53	77/53
χ^2(diff)/ndf	52/60	54/60	45/60	59/60	71/60	73/60

polynomial is set to a quadratic function; in the third alternative, the mean of the hyperbolic tangent is allowed to be a free parameter, rather than being constrained to the mean D^- mass;

(iv) for the μD^* channel, the mass window used to select $D^0 \to K\pi$ candidates is varied, from the nominal requirement of $1.7 < M(K\pi) < 2.0$ GeV$/c^2$, to 12 alternative ranges, giving different background fractions and shapes in the final distribution;

(v) the function $F^{\rm sig}$, used to model the signal shape, is changed to an alternative choice; for the μD case, a single Gaussian function is used; for the μD^* case, a skewed double-Gaussian is used;

(vi) the function $F^{\rm BG}_{\rm diff}$, used to model the background of the difference distribution, is changed to an alternative choice; for the μD case, a linear function is used; for the μD^* case, a second or fourth order polynomial is used;

(vii) the event weights are allocated using an alternative method, based on the fitted number of $\mu D^{(*)}$ signal events in each polarity configuration, rather than the total number of candidates.

To properly assess the combined effect of all these adjustments to the fit, including correlations, all possible combinations of the above fit variations are tested, and the systematic uncertainty is allocated as the standard deviation of the full set of alternative measurements. Table III shows the final systematic uncertainties allocated for each VPDL bin, for both channels. The combined systematic uncertainty is significantly smaller than the statistical uncertainty in all cases.

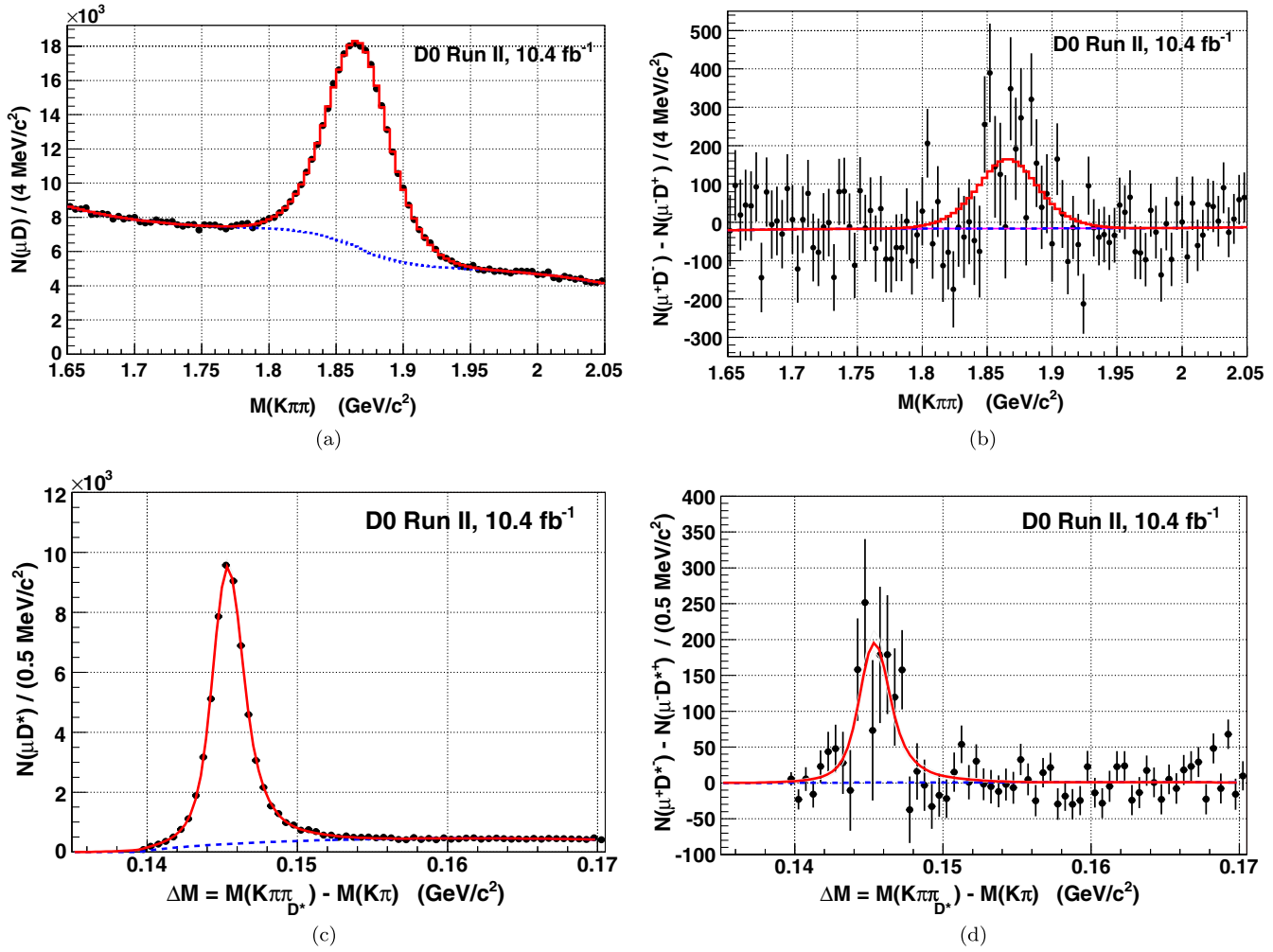

FIG. 3 (color online). Examples of the raw asymmetry fit for the two decays channels, for the fifth VPDL(B^0) bin corresponding to ($0.10 <$ VPDL(B^0) < 0.20) cm. The left plots show the sum distributions; the right plots show the difference distributions. In both cases, the solid line represents the total fit function, with the background part shown separately by the dashed line (see text). (a) $H_{\rm sum}(\mu D$ channel); (b) $H_{\rm diff}(\mu D$ channel); (c) $H_{\rm sum}(\mu D^*$ channel); (d) $H_{\rm diff}(\mu D^*$ channel).

TABLE III. Systematic uncertainties on the raw asymmetry measurement for both channels, extracted from an ensemble of fits with variations on each quantity tested. Also shown are the corresponding statistical uncertainties, for comparison.

Source	Bin 1 −0.10–0.00 cm	Bin 2 0.00–0.02 cm	Bin 3 0.02–0.05 cm	Bin 4 0.05–0.10 cm	Bin 5 0.10–0.20 cm	Bin 6 0.20–0.60 cm
			μD channel			
Bin width	0.09%	0.01%	0.01%	0.01%	0.00%	0.05%
Fit limits	0.17%	0.06%	0.08%	0.05%	0.03%	0.12%
Magnet weighting	0.02%	0.00%	0.00%	0.00%	0.00%	0.01%
Signal model	0.03%	0.03%	0.01%	0.04%	0.01%	0.01%
Background model (sum)	0.03%	0.00%	0.01%	0.01%	0.01%	0.00%
Background model (diff)	0.01%	0.00%	0.01%	0.00%	0.01%	0.02%
Combined systematic	±0.19%	±0.07%	±0.08%	±0.07%	±0.05%	±0.13%
Statistical	±1.28%	±0.35%	±0.32%	±0.33%	±0.41%	±0.88%
			μD^* channel			
Bin width	0.06%	0.03%	0.02%	0.02%	0.01%	0.08%
Fit limits	0.05%	0.01%	0.01%	0.01%	0.06%	0.06%
Magnet weighting	0.01%	0.01%	0.00%	0.00%	0.00%	0.01%
Signal model	0.01%	0.01%	0.05%	0.06%	0.03%	0.03%
Background model	0.13%	0.01%	0.00%	0.01%	0.07%	0.01%
M(D^0) cut	0.01%	0.01%	0.01%	0.01%	0.02%	0.02%
Combined systematic	±0.13%	±0.04%	±0.05%	±0.07%	±0.08%	±0.09%
Statistical	±0.67%	±0.30%	±0.30%	±0.33%	±0.44%	±0.99%

VII. ACCOUNTING FOR DETECTOR ASYMMETRIES

Both channels used in this measurement are reconstructed from the final state particles $\mu^{\pm}K^{\pm}\pi^{\mp}\pi^{\mp}$. In relating the measured raw asymmetry to the physical asymmetry under investigation, the effects of possible charge asymmetries in particle reconstruction must be considered. Neglecting asymmetries of second order or higher, the background asymmetry simplifies to

$$A_{\mathrm{BG}} = a^{\mu} + a^{K} - 2a^{\pi}, \tag{29}$$

where the asymmetries a^X are defined as the difference in reconstruction efficiency ε for the positively and negatively charged particles:

$$a^X \equiv \frac{\varepsilon^{X^+} - \varepsilon^{X^-}}{\varepsilon^{X^+} + \varepsilon^{X^-}}. \tag{30}$$

A. Kaon asymmetry

By far the largest background asymmetry to be taken into account is due to differences in the behavior of positive and negative kaons as they traverse the detector. Negative kaons can interact with matter in the tracking system to produce hyperons, while there is no equivalent interaction for positive kaons. As a result, the mean path length for positive kaons is longer, the reconstruction efficiency is higher, and the kaon asymmetry a^K is positive.

The kaon asymmetry is measured using a dedicated sample of $K^{*0} \to K^+\pi^-$ decays, based on the technique described in Ref. [30]. The $K^+\pi^-$ and $K^-\pi^+$ signal yields are extracted by fitting the charge-specific $M(K^{\pm}\pi^{\mp})$ distributions, and the asymmetry is determined by dividing the difference by the sum. The track selection criteria are the same as those required for the $\mu D^{(*)}$ signal channels, and all events must contain a muon passing the selections described in Sec. IV. Since the K^{*0} channel includes a final state pion, of opposite charge to the kaon, the correction will also absorb any tracking asymmetry affecting pion reconstruction. One of the two a^{π} terms in Eq. (29) is eliminated as a result.

As expected, an overall positive kaon asymmetry is observed, of approximately 1% in this channel. A strong dependence on kaon momentum and absolute

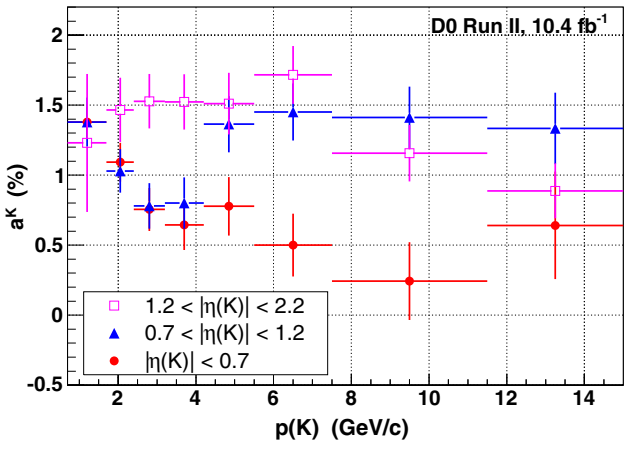

FIG. 4 (color online). Kaon asymmetry as a function of kaon momentum, for three regions of absolute pseudorapidity, as extracted from the $K^{*0} \to K^+\pi^-$ channel.

TABLE IV. Kaon charge asymmetries in bins of $p(K)$, as extracted from the $K^{*0} \to K^+\pi^-$ channel, for each of the three regions in absolute pseudorapidity: central ($|\eta(K)| < 0.7$); midrange ($0.7 \leq |(K)| < 1.2$); and forward ($1.2 \leq |\eta(K)| < 2.2$).

	a^K (%)		
$p(K)$ range	Central	Midrange	Forward
0.7–1.7	1.38 ± 0.11	1.38 ± 0.18	1.23 ± 0.49
1.7–2.4	1.09 ± 0.14	1.03 ± 0.16	1.47 ± 0.23
2.4–3.2	0.76 ± 0.15	0.78 ± 0.16	1.53 ± 0.20
3.2–4.2	0.65 ± 0.18	0.80 ± 0.18	1.52 ± 0.20
4.2–5.5	0.78 ± 0.21	1.36 ± 0.20	1.51 ± 0.22
5.5–7.5	0.50 ± 0.22	1.45 ± 0.20	1.72 ± 0.21
7.5–11.5	0.24 ± 0.28	1.41 ± 0.22	1.16 ± 0.20
≥ 11.5	0.64 ± 0.38	1.33 ± 0.26	0.89 ± 0.20

pseudorapidity is found, and hence the final kaon asymmetry correction to be applied in Eq. (29) is determined by the weighted average of $a^K[p(K), |\eta(K)|]$ over the $p(K)$ and $|\eta(K)|$ distributions in the signal events:

$$a^K = \sum_{i=1}^{24} a_i^K \cdot \left(\frac{N_i^K}{N}\right), \tag{31}$$

where the sum is over eight bins in kaon momentum multiplied by three bins in absolute pseudorapidity, and N is the total number of signal candidates over all bins. The kaon asymmetry as a function of momentum is shown in Fig. 4 for each of the three $|\eta(K)|$ regions, and the values and bin definitions are listed in Table IV. A relative systematic uncertainty of 5% is assigned to each bin to account for possible variations in the yield when different models are used to fit the signal and backgrounds in the K^{*0} mass distribution.

The kaon momentum distributions for each channel, within each $|\eta(K)|$ region, and for each VPDL(B^0) bin, are determined by fitting the appropriate invariant mass distribution in each of the eight kaon momentum bins, using the same parametrizations F_{sum} as described in Sec. VI. Following studies over a range of fit variations, a relative systematic uncertainty of 3% (0.5%) is assigned on all μD (μD^*) yields.

The final corrections for each VPDL bin in both channels are presented in Table V. The kaon corrections for the μD^* channel are slightly smaller than for the μD channel, due to different kaon kinematics in the two decay topologies.

B. Track asymmetry

Unlike kaons, positive and negative pions have almost identical interaction cross sections in matter. Any possible asymmetry will be dominated by effects from track detection and reconstruction, which should be removed to first order by the magnet polarity weighting.

The transverse momentum dependence of any residual tracking asymmetry is studied in $K_S^0 \to \pi^+\pi^-$ decays. This channel can only be observed if a pair of oppositely charged pions is reconstructed, hence it is insensitive to the absolute asymmetry, and the overall scale is arbitrarily fixed by setting the asymmetry in the lowest p_T bin to zero. The relative asymmetry as a function of p_T is determined by extracting the K_S^0 yields in bins of $[p_T(\pi^+), p_T(\pi^-)]$, and following the method described in Ref. [30], except that $K_S^0 \to \pi^+\pi^-$ decays are used instead of $J/\psi \to \mu^+\mu^-$. As shown in Fig. 5, no evidence of any track p_T dependence is observed, over the range 0.5–7 GeV/c, within an uncertainty of ±0.05%. As a result, any residual tracking asymmetry will cancel to first order in the reconstruction of the pion and oppositely charged muon, which remain to be taken into account after applying the kaon asymmetry correction. There are insufficient statistics in the $K_S^0 \to \pi^+\pi^-$ channel to extend to higher transverse momenta. However, this momentum region contains the majority of $\mu D^{(*)}$ signal candidates.

A second dedicated channel $K^{\pm *} \to K_S^0\pi^\pm$ is used to measure the absolute residual track asymmetry. The $K_S^0\pi^\pm$ yields for each pion charge are extracted by fitting the

TABLE V. The background asymmetries from kaon and muon reconstruction, in bins of VPDL(B^0), for both signal channels. Also shown are the raw asymmetries A, and the combined background asymmetries $A_{\text{BG}} = a^K + a^\mu - 2a^\pi$, where the final term contributes no net asymmetry but a systematic uncertainty of ±0.05%. In each case, the first uncertainty is statistical, the second systematic.

	Bin 1 −0.10–0.00 cm	Bin 2 0.00–0.02 cm	Bin 3 0.02–0.05 cm	Bin 4 0.05–0.10 cm	Bin 5 0.10–0.20 cm	Bin 6 0.20–0.60 cm
			μD channel			
A (%)	2.70 ± 1.28 ± 0.19	1.02 ± 0.35 ± 0.07	1.16 ± 0.32 ± 0.08	1.50 ± 0.33 ± 0.07	1.48 ± 0.41 ± 0.05	1.20 ± 0.88 ± 0.13
a^K (%)	1.128 ± 0.041 ± 0.014	1.124 ± 0.040 ± 0.014	1.141 ± 0.040 ± 0.014	1.147 ± 0.040 ± 0.014	1.157 ± 0.040 ± 0.015	1.157 ± 0.040 ± 0.014
a^μ (%)	0.102 ± 0.025 ± 0.008	0.105 ± 0.027 ± 0.009	0.107 ± 0.029 ± 0.012	0.107 ± 0.029 ± 0.013	0.108 ± 0.028 ± 0.011	0.108 ± 0.028 ± 0.009
A_{BG} (%)	1.230 ± 0.048 ± 0.053	1.229 ± 0.048 ± 0.053	1.248 ± 0.049 ± 0.053	1.254 ± 0.049 ± 0.054	1.265 ± 0.049 ± 0.053	1.265 ± 0.049 ± 0.053
			μD^* channel			
A (%)	1.82 ± 0.67 ± 0.13	1.10 ± 0.30 ± 0.04	0.94 ± 0.30 ± 0.05	1.38 ± 0.33 ± 0.07	2.11 ± 0.44 ± 0.08	0.55 ± 0.99 ± 0.09
a^K (%)	1.089 ± 0.047 ± 0.013	1.078 ± 0.052 ± 0.014	1.078 ± 0.050 ± 0.014	1.085 ± 0.050 ± 0.014	1.086 ± 0.049 ± 0.014	1.098 ± 0.050 ± 0.014
a^μ (%)	0.097 ± 0.027 ± 0.012	0.098 ± 0.031 ± 0.022	0.101 ± 0.033 ± 0.023	0.101 ± 0.033 ± 0.022	0.101 ± 0.033 ± 0.020	0.101 ± 0.031 ± 0.016
A_{BG} (%)	1.186 ± 0.054 ± 0.053	1.176 ± 0.061 ± 0.056	1.179 ± 0.060 ± 0.057	1.186 ± 0.060 ± 0.056	1.187 ± 0.059 ± 0.056	1.199 ± 0.059 ± 0.054

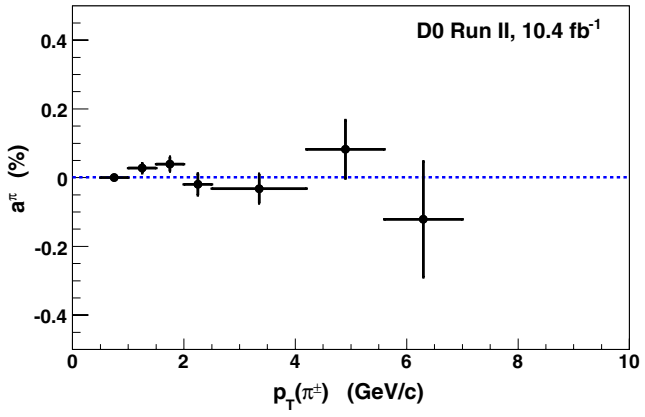

FIG. 5 (color online). Relative track reconstruction asymmetry as a function of track transverse momentum, as measured from $K^0_S \to \pi^+\pi^-$ decays. The absolute scale is chosen to give zero asymmetry for the first bin, since this channel is only sensitive to the variations in asymmetry between bins.

$M(K^0_S\pi^\pm)$ invariant mass distributions, and the asymmetry calculated from the sum and difference of these yields. No significant asymmetry is found in this study, which is consistent with the findings of previous studies [30]. As such, no correction is applied to the asymmetry to account for the effects of track reconstruction, and a^π in Eq. (29) is assigned to be zero. We allocate a systematic uncertainty of $\pm 0.05\%$ to account for the limited precision of this asymmetry measurement.

C. Muon asymmetry

The residual charge asymmetry for muon identification is measured using $J/\psi \to \mu^+\mu^-$ decays, using the technique developed in Ref. [30]. A small but significant asymmetry is observed, with a sizeable dependence on the muon transverse momentum, as shown in Fig. 6. The corresponding correction a^μ to be applied to the raw asymmetry is extracted using the same method as for the kaon asymmetry, by performing a weighted average of the muon asymmetry over bins of $p_T(\mu)$, analogous to Eq. (31).

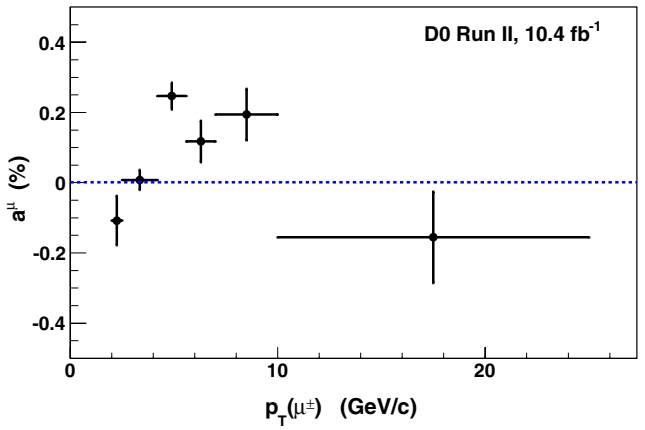

FIG. 6 (color online). Muon asymmetry as a function of muon transverse momentum, as extracted from a dedicated sample of $J/\psi \to \mu^+\mu^-$ decays.

The final muon asymmetry corrections for each VPDL bin and both channels are summarized in Table V. To account for possible systematic uncertainties, the entire procedure of measuring muon asymmetries and convoluting with the transverse momentum distributions is repeated with several variations to the method, and the corresponding changes in the final measured muon asymmetry in each bin are used to assign a systematic uncertainty. The variations include changing the mass binning of the $M(\mu^+\mu^-)$ distributions, changing the fitting function used to extract the J/ψ yields, changing the p_T binning scheme, including an absolute pseudorapidity dependence, and using an alternative method to determine the polarity-based event weights.

VIII. SAMPLE COMPOSITION: DILUTION FROM SYMMETRIC PROCESSES

Not all $\mu D^{(*)}$ combinations originate from the decay of oscillated B^0 mesons. Alternative charge-symmetric sources will contribute only to the denominator in the raw asymmetry extraction, and hence dilute any physical asymmetry $a^d_{\rm sl}$.

In general, mesons containing a charm quark can be produced in many different ways, which we divide into five categories for the purposes of this measurement:

(1) direct hadronization from an initial $c(\bar{c})$ quark, here denoted as "prompt";
(2) as a product of B^0 meson decay;
(3) as a product of $B^\pm$ meson decay;
(4) as a product of B^0_s meson decay; and
(5) as a product of a b baryon decay.

The contribution from b baryons is found to be negligible, using the technique described below, and will no longer be considered. This scheme includes possible intermediate excited resonances of both B and D mesons, for example, processes such as $c \to D^{*0}X \to D^+X'$ or those with higher excitations. For both neutral B meson sources, there may be mixing via box diagrams prior to decay, so sources 2 and 4 in the above list can be subdivided into "mixed" and "direct" decays.

The total fraction of signal events coming from B^0 meson decays is determined using inclusive MC simulations in which the only requirement at the generator level is the presence of the appropriate $D^{(*)\mp}$ decay channel, and the presence of a muon (of any charge). The samples include nonprimary gluon splitting into heavy flavor $b\bar{b}$ and $c\bar{c}$ pairs, in addition to pair production from flavor excitation and flavor creation mechanisms. The generated events are passed through the full simulation chain, and then processed by the same reconstruction and selection

algorithms as used to select events from real data for the two signal channels.

At the reconstruction level, the final state tracks must correspond to the true kaons and pions from the $D^{(*)\mp}$ decay. The result for each channel is a sample of $D^{(*)\mp}$ events, with an accompanying reconstructed muon, in which the decay chain can be investigated in detail to extract the parentage information. The candidates are weighted according to their true decay time, to ensure that the B meson lifetimes match the current world-average measurements, with the uncertainties on these lifetimes taken into account when assigning systematic uncertainties.

Table VI lists the resulting fractions of $\mu D^{(*)}$ candidates from each source in both signal channels, as a function of the reconstructed VPDL(B^0). In general, the B^0 fraction is approximately 80%–90%, except in the first (negative VPDL) bin in which the prompt contribution reduces this to around 60%. The $B^{\pm}$ contribution is small but significant, building from approximately 5%–18% (6%–14%) in the $\mu D^{(*)}$ case as the VPDL increases. This graduation is due to the longer lifetime of the $B^{\pm}$ meson relative to B^0.

For all bins, the B_s^0 fraction is very small, at approximately 1%–3%. We correct for the possible contribution from the semileptonic mixing asymmetry in B_s^0 mesons, $a_{\rm sl}^s$, on a VPDL bin-by-bin basis, by extending Eq. (9) to include the nonzero B_s^0 fraction:

$$a_{\rm sl}^d = \frac{A - A_{\rm BG} - F_{B_s^0}^{\rm osc} \cdot a_{\rm sl}^s}{F_{B^0}^{\rm osc}}. \tag{32}$$

Here $F_{B_s^0}^{\rm osc} = F(B_s^0 \to \mu D^{(*)} X) \cdot \chi_s$ is the fractional contribution of oscillated B_s^0 mesons in the sample, where $\chi_s = 0.499\,292 \pm 0.000\,016$ is the integrated mixing probability [6]. The parameter $a_{\rm sl}^s$ is assigned the world-average value, $[-1.05 \pm 0.64]\%$ [6]. The uncertainty on this quantity is taken into account when determining the systematic uncertainty on the final measurement.

The fraction of B^0 mesons that oscillate into their antiparticle prior to decay is determined by applying a weight $W_j^{\rm mix}$ to all $B^0 \to \mu D^{(*)}$ events based on the true decay time (t_j) of the B^0 meson:

$$W_j^{\rm mix} = \frac{1}{2}[1 - \cos(\Delta M_d \cdot t_j)], \tag{33}$$

where ΔM_d is the mass difference of the heavy and light eigenstates in the B^0 system, assigned to be the world-average value $0.507 \pm 0.004\ {\rm ps}^{-1}$ [6], with the precision taken into account when assigning systematic uncertainties. The resulting fractions $F_{B^0}^{\rm osc}$ are defined as the sum of these mixing weights divided by the total number of events in the MC sample. Table VI lists the resulting fractions versus VPDL for both channels.

Various sources of systematic uncertainty on $F_{B^0}^{\rm osc}$ are considered. The prompt fraction is negligible in VPDL bins 3–6 used in the final $a_{\rm sl}^d$ measurement; therefore, no systematic uncertainties are allocated from this source.

The simulation may not describe the data perfectly. In particular, the simulation does not account for any effects due to the muon triggers used to collect data. MC simulations show that the pretrigger muon transverse momenta distributions from B^0 and $B^{\pm}$ decays are completely consistent, as expected from the closeness of the meson masses. On the other hand, there are small differences in the $p_T(\mu)$ distributions for B_s^0 decays. Reweighting events by a trigger acceptance correction leads to a small reduction in the B_s^0 fraction, of order 3%. Since this source accounts for less than 3% of all $D^{(*)-}$ candidates, the effect of this trigger correction on $F_{B^0}^{\rm osc}$ is tiny, of order 0.001, and is neglected.

The decay branching ratios of B^0 mesons into semileptonic final states containing a $D^{\mp}$ ($D^{*\mp}$) meson are known to around 10% (5%) precision [6]. As such, we vary the B^0 fractions up and down for the two channels by these fractions and assign a systematic uncertainty from

TABLE VI. Fraction of $D^{(*)\pm}$ candidates arising from each source as determined from MC simulation, for both channels, and in bins of VPDL(B^0). For each channel, the first row lists the central values and statistical uncertainties (from limited sample size in simulation), while the second row lists the systematic uncertainties, only determined for the final $F_{B^0}^{\rm osc}$ values.

	Bin 1 −0.10–0.00 cm	Bin 2 0.00–0.02 cm	Bin 3 0.02–0.05 cm	Bin 4 0.05–0.10 cm	Bin 5 0.10–0.20 cm	Bin 6 0.20–0.60 cm
			μD channel			
$F(\bar{c} \to \mu D X)$	0.361 ± 0.011	0.069 ± 0.003	0.003 ± 0.000	0.000 ± 0.000	0.000 ± 0.000	0.000 ± 0.000
$F(B_s^0 \to \mu D X)$	0.019 ± 0.003	0.019 ± 0.001	0.029 ± 0.001	0.027 ± 0.001	0.030 ± 0.002	0.032 ± 0.004
$F(B^{\pm} \to \mu D X)$	0.052 ± 0.005	0.075 ± 0.003	0.101 ± 0.003	0.118 ± 0.003	0.141 ± 0.004	0.186 ± 0.008
$F(B^0 \to \mu D X)$	0.569 ± 0.011	0.837 ± 0.004	0.868 ± 0.003	0.854 ± 0.003	0.829 ± 0.004	0.781 ± 0.009
$F_{B^0}^{\rm osc}$	$0.018 \pm 0.003 \pm 0.001$	$0.009 \pm 0.001 \pm 0.000$	$0.057 \pm 0.002 \pm 0.001$	$0.208 \pm 0.003 \pm 0.005$	$0.520 \pm 0.005 \pm 0.011$	$0.658 \pm 0.010 \pm 0.017$
			μD^* channel			
$F(\bar{c} \to \mu D^* X)$	0.373 ± 0.010	0.082 ± 0.003	0.005 ± 0.001	0.000 ± 0.000	0.001 ± 0.000	0.000 ± 0.000
$F(B_s^0 \to \mu D^* X)$	0.009 ± 0.002	0.011 ± 0.001	0.014 ± 0.001	0.013 ± 0.001	0.016 ± 0.002	0.017 ± 0.005
$F(B^{\pm} \to \mu D^* X)$	0.058 ± 0.005	0.073 ± 0.003	0.080 ± 0.003	0.083 ± 0.003	0.104 ± 0.005	0.146 ± 0.013
$F(B^0 \to \mu D^* X)$	0.560 ± 0.010	0.835 ± 0.004	0.901 ± 0.003	0.903 ± 0.004	0.880 ± 0.005	0.836 ± 0.013
$F_{B^0}^{\rm osc}$	$0.013 \pm 0.002 \pm 0.001$	$0.010 \pm 0.001 \pm 0.000$	$0.061 \pm 0.003 \pm 0.002$	$0.231 \pm 0.005 \pm 0.003$	$0.570 \pm 0.008 \pm 0.007$	$0.713 \pm 0.016 \pm 0.008$

TABLE VII. Systematic uncertainties from different sources on the dilution fraction $F^{\rm osc}_{B^0}$, for both channels, and in bins of VPDL(B^0).

	Bin 1 -0.10–0.00 cm	Bin 2 0.00–0.02 cm	Bin 3 0.02–0.05 cm	Bin 4 0.05–0.10 cm	Bin 5 0.10–0.20 cm	Bin 6 0.20–0.60 cm
			$F^{\rm osc}_{B^0}(\mu D)$			
Branching ratios	±0.001	±0.000	±0.001	±0.004	±0.009	±0.015
B meson lifetimes	±0.000	±0.000	±0.000	±0.001	±0.003	±0.007
ΔM_d	±0.000	±0.000	±0.001	±0.003	±0.005	±0.002
Total	±0.001	±0.000	±0.001	±0.005	±0.011	±0.017
			$F^{\rm osc}_{B^0}(\mu D^*)$			
Branching ratios	±0.001	±0.000	±0.001	±0.001	±0.004	±0.006
B meson lifetimes	±0.000	±0.000	±0.001	±0.001	±0.003	±0.005
ΔM_d	±0.000	±0.000	±0.001	±0.003	±0.005	±0.003
Total	±0.001	±0.000	±0.002	±0.003	±0.007	±0.008

this source equal to the total variation with respect to the default value.

To account for the uncertainties on the world-average B meson lifetime values, we repeat the evaluation of $F^{\rm osc}_{B^0}$ with the input lifetimes adjusted within their uncertainties, and assign a systematic uncertainty equal to the maximum deviation from the nominal $F^{\rm osc}_{B^0}$ value. Similarly, systematic uncertainties are allocated to account for the limited precision of ΔM_d and $a^s_{\rm sl}$. The breakdown of systematic uncertainties is shown in Table VII. For the final measurement of $a^d_{\rm sl}$, the uncertainties from the limited sample size in simulation are also categorized as systematic, not statistical, since they are not related to the size of the data sample.

IX. RESULTS

From the raw asymmetries and detector-related asymmetries listed in Table V, and the corresponding dilution fractions $F^{\rm osc}_{B^0}$ presented in Table VI, the final value of the semileptonic mixing asymmetry $a^d_{\rm sl}$ is determined for each VPDL bin $i = \{3, 4, 5, 6\}$, and for each channel $j = \{\mu D, \mu D^*\}$:

$$a^d_{\rm sl}(ij) = \frac{A(ij) - a^K(ij) - a^\mu(ij) - F^{\rm osc}_{B^0_s}(ij) \cdot a^s_{\rm sl}}{F^{\rm osc}_{B^0}(ij)}. \quad (34)$$

The first two VPDL bins, $i = \{1, 2\}$ are not included, as these represent the control region in which the expected signal contribution is negligible.

To extract the corresponding uncertainties (both statistical and systematic) care must be taken to properly account for all the correlations and constraints on the various inputs to the measurement. In particular,

(i) the raw asymmetries for each bin and channel are independent;
(ii) the kaon asymmetry as a function of $[p(K), |\eta(K)|]$ (Fig. 4) is 100% correlated between bins, and between channels;
(iii) the muon asymmetry as a function of $p_T(\mu)$ (Fig. 6) is 100% correlated between bins, and between channels;
(iv) the asymmetry $a^s_{\rm sl}$, used to derive the correction for a possible contribution from B^0_s mixing, is 100% correlated between bins, and between channels;
(v) the oscillation fractions, $F^{\rm osc}_{B^0}$, are treated as independent.

While we expect some correlations between bins, and between channels, in the oscillated B^0 fractions $F^{\rm osc}_{B^0}$, studies indicate that their effect on the final $a^d_{\rm sl}$ measurement is negligible, justifying their exclusion.

To ensure that all such correlations are taken into account, the final statistical and systematic uncertainties on each $a^d_{\rm sl}$ measurement, and on the combination, are derived from 200 000 ensemble tests in which all input variables are randomly chosen according to a Gaussian probability density function, with an appropriate central value and width, and the distributions of the resulting $a^d_{\rm sl}$ measurements are inspected and fitted. This process is performed twice, once with the inputs varied according to their statistical uncertainties, and once with the inputs varied according to their systematic uncertainties.

Figure 7 and Table VIII show the individual results for the four signal VPDL bins in each channel, with statistical and systematic uncertainties.

Once the uncertainties on the individual $a^d_{\rm sl}$ measurements are established, the combination between VPDL bins, and then between channels, is performed. For each channel, the combined $a^d_{\rm sl}$ value is obtained by a weighted average of the four individual measurements:

$$a^d_{\rm sl}(j) = \frac{\sum_{i=3}^{6} a^d_{\rm sl}(ij) w(ij)}{\sum_{i=3}^{6} w(ij)}, \quad (35)$$

where the weights $w(ij)$ are the inverse of the sum in quadrature of statistical and systematic uncertainties for that measurement:

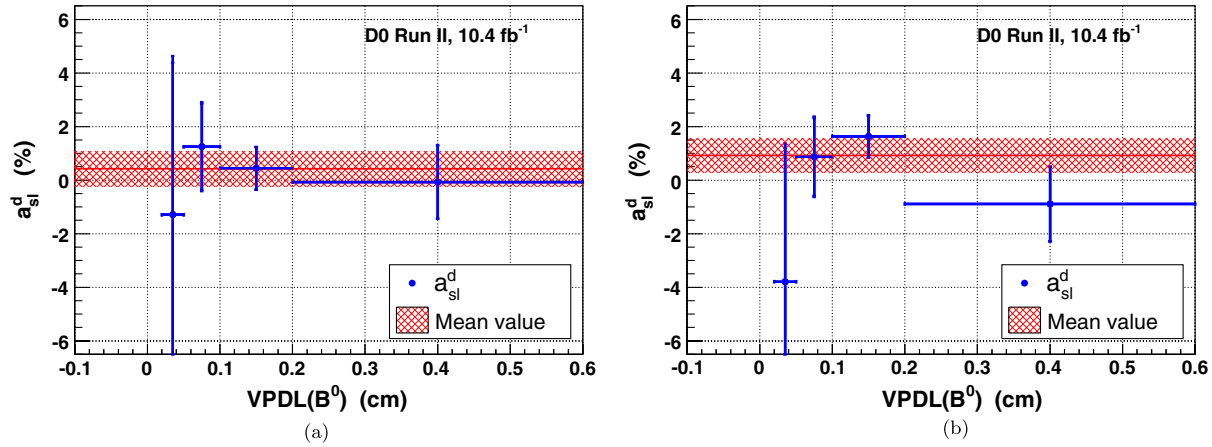

FIG. 7 (color online). Final measurements of the semileptonic asymmetry $a^d_{\rm sl}$, in bins of VPDL(B^0), for both channels. The cross-hatched bands show the mean values (and their total uncertainties) determined for each channel separately. (a) μD channel; (b) μD^* channel.

$$w(ij) = \frac{1}{\sigma^2_{\rm stat}[a^d_{\rm sl}(ij)] + \sigma^2_{\rm syst}[a^d_{\rm sl}(ij)]}. \quad (36)$$

The central values and uncertainties for the combinations are again determined by performing the full set of 200 000 ensemble tests, with all inputs varied, and examining the effect on the final values of $a^d_{\rm sl}$ from each channel. This procedure yields the following results:

$$a^d_{\rm sl}(\mu D) = [0.43 \pm 0.63({\rm stat}) \pm 0.16({\rm syst})]\%, \quad (37)$$

$$a^d_{\rm sl}(\mu D^*) = [0.92 \pm 0.62({\rm stat}) \pm 0.16({\rm syst})]\%. \quad (38)$$

Finally, the combination is extended to give the full weighted average of the two channel-specific measurements, with full propagation of uncertainties, to yield the final measurement:

$$a^d_{\rm sl} = [0.68 \pm 0.45({\rm stat}) \pm 0.14({\rm syst})]\%. \quad (39)$$

The weights $w(ij)$ used for this combination are presented in Table VIII.

X. CROSS-CHECKS

To test the robustness of the measurement technique, the analysis is repeated with the event samples divided into pairs of orthogonal subsets, of approximately equal size. The raw asymmetries A, detector-related background corrections a^K and a^μ, and oscillation fractions $F^{\rm osc}_{B^0}$ are redetermined for each subsample, and the semileptonic mixing asymmetry $a^d_{\rm sl}$ measured in each case. The subsamples are defined by the following criteria:

(i) $\eta(\mu) < 0$ and $\eta(\mu) > 0$;
(ii) $|\eta(K)| < 0.7$ and $|\eta(K)| > 0.7$;
(iii) $p(K) < 3.2$ GeV/c and $p(K) > 3.2$ GeV/c;
(iv) a chronological division corresponding to early and late data collection;
(v) $\sigma({\rm VPDL}) < 40$ μm and $\sigma({\rm VPDL}) > 40$ μm.

The results are summarized in Table IX. In all cases, the measured values of $a^d_{\rm sl}$ are statistically consistent with each other, despite some samples having significantly different background corrections.

TABLE VIII. Individual measurements of $(A - A_{\rm BG})$ and $a^d_{\rm sl}$ in each of the six VPDL(B^0) bins, for both channels in this analysis. For each entry, the first uncertainty is statistical, the second systematic, with all correlations taken into account. Also shown are the weights $w(ij)$ used to combine the eight separate measurements, normalized to unity.

	Bin 1 −0.10–0.00 cm	Bin 2 0.00–0.02 cm	Bin 3 0.02–0.05 cm	Bin 4 0.05–0.10 cm	Bin 5 0.10–0.20 cm	Bin 6 0.20–0.60 cm
			μD Channel			
$A - A_{\rm BG}$ (%)	$1.48 \pm 1.28 \pm 0.20$	$-0.20 \pm 0.35 \pm 0.09$	$-0.07 \pm 0.32 \pm 0.10$	$0.26 \pm 0.33 \pm 0.09$	$0.23 \pm 0.41 \pm 0.07$	$-0.05 \pm 0.89 \pm 0.14$
$a^d_{\rm sl}$ (%)	Not used		$-1.29 \pm 5.68 \pm 1.69$	$1.25 \pm 1.61 \pm 0.43$	$0.44 \pm 0.79 \pm 0.14$	$-0.07 \pm 1.36 \pm 0.21$
weight $w(ij)/\sum_{ij} w(ij)$	Not used		0.006	0.072	0.309	0.105
			μD^* Channel			
$A - A_{\rm BG}$ (%)	$0.64 \pm 0.67 \pm 0.14$	$-0.07 \pm 0.31 \pm 0.07$	$-0.23 \pm 0.31 \pm 0.08$	$0.20 \pm 0.34 \pm 0.09$	$0.93 \pm 0.44 \pm 0.10$	$-0.63 \pm 0.99 \pm 0.11$
$a^d_{\rm sl}$ (%)	Not used		$-3.79 \pm 5.00 \pm 1.27$	$0.87 \pm 1.45 \pm 0.39$	$1.63 \pm 0.78 \pm 0.17$	$-0.89 \pm 1.39 \pm 0.15$
weight $w(ij)/\sum_{ij} w(ij)$	Not used		0.007	0.088	0.311	0.102

TABLE IX. Results of the analysis cross-checks, in which the data are divided into pairs of orthogonal and independent subsets, and the measurements of $a^d_{\rm sl}$ repeated for each sample. The uncertainties shown here are the sum in quadrature of the statistical and systematic components.

Subsample requirement	$a^d_{\rm sl}$ (%) μD channel	μD^* channel	Comb.
Nominal result	0.43 ± 0.65	0.92 ± 0.64	0.68 ± 0.47
$\eta(\mu) < 0$	0.38 ± 0.88	0.60 ± 0.88	0.49 ± 0.63
$\eta(\mu) > 0$	0.53 ± 0.91	1.21 ± 0.88	0.88 ± 0.64
$\lvert\eta(K)\rvert < 0.7$	0.48 ± 0.95	-0.39 ± 1.14	0.04 ± 0.77
$\lvert\eta(K)\rvert > 0.7$	0.36 ± 0.85	1.17 ± 0.86	0.76 ± 0.62
$p(K) < 3.2$ GeV/c	0.02 ± 0.87	-0.30 ± 1.42	-0.14 ± 0.85
$p(K) > 3.2$ GeV/c	1.11 ± 0.92	1.00 ± 0.79	1.05 ± 0.62
σ(VPDL) < 40 μm	0.22 ± 0.84	0.18 ± 0.95	0.20 ± 0.65
σ(VPDL) > 40 μm	0.76 ± 0.95	0.98 ± 1.01	0.87 ± 0.70
First half data	0.82 ± 0.89	1.39 ± 0.88	1.11 ± 0.67
Second half data	0.19 ± 0.86	-0.30 ± 1.02	-0.06 ± 0.68

In addition, the measurement is repeated using only events that satisfy a single muon trigger. This corresponds to approximately 90% of the total sample. The resulting $a^d_{\rm sl}$ value for these events is consistent with the nominal value, taking into account the correlation between the samples.

The fraction of events from mixed B^0 decays, $F^{\rm osc}_{B^0}$, is a strong function of the visible proper decay length of the reconstructed B^0 candidate. Hence any nonzero value of $a^d_{\rm sl}$ will lead to a VPDL dependence on the background-subtracted asymmetry $(A - A_{\rm BG})$ [see Eq. (6)]. Figure 8 shows this dependence for both channels, with the $F^{\rm osc}_{B^0} \cdot a^d_{\rm sl}$ distribution superimposed on the plot for comparison, using the final $a^d_{\rm sl}$ measurement from the two channel combination. The two distributions are statistically consistent, indicating that the VPDL dependence of the observed background-subtracted asymmetry is consistent with the hypothesis that it originates from the mixing of B^0 mesons.

The χ^2 quantifying this agreement between the $(A - A_{\rm BG})$ and $F^{\rm osc}_{B^0} \cdot a^d_{\rm sl}$ distributions is 2.3 (4.5) for the $\mu D^{(*)}$ channel, compared to 2.7 (6.9) under the SM assumption for $a^d_{\rm sl}$. For this test, the statistical and systematic uncertainties are combined in quadrature.

The same data can be used to validate the $a^d_{\rm sl}$ measurement using an alternative method, in which the distribution of $(A - A_{\rm BG})$ versus VPDL(B^0) is fitted to the function:

$$F(\text{VPDL}) = A_{\rm const} + F^{\rm osc}_{B^0}(\text{VPDL}) \cdot a^d_{\rm sl}, \tag{40}$$

where $a^d_{\rm sl}$ and $A_{\rm const}$ are the two free parameters. The constant asymmetry term allows for a contribution from possible additional background sources of asymmetry that have not been considered in this analysis. For this study we neglect any uncertainties on $F^{\rm osc}_{B^0}$. The results are as follows:

$$a^d_{\rm sl} = (0.51 \pm 0.86)\% \ (\mu D \text{ channel}), \tag{41}$$

$$a^d_{\rm sl} = (1.25 \pm 0.87)\% \ (\mu D^* \text{ channel}). \tag{42}$$

These values are consistent with those from the full analysis method. The uncertainties are larger as a result of the additional parameter in the fit. The constant asymmetry parameter converges to values consistent with zero for both channels:

$$A_{\rm const} = (-0.03 \pm 0.23)\% \ (\mu D \text{ channel}), \tag{43}$$

$$A_{\rm const} = (-0.09 \pm 0.21)\% \ (\mu D^* \text{ channel}), \tag{44}$$

demonstrating that any possible residual background asymmetries not accounted for are small, as expected.

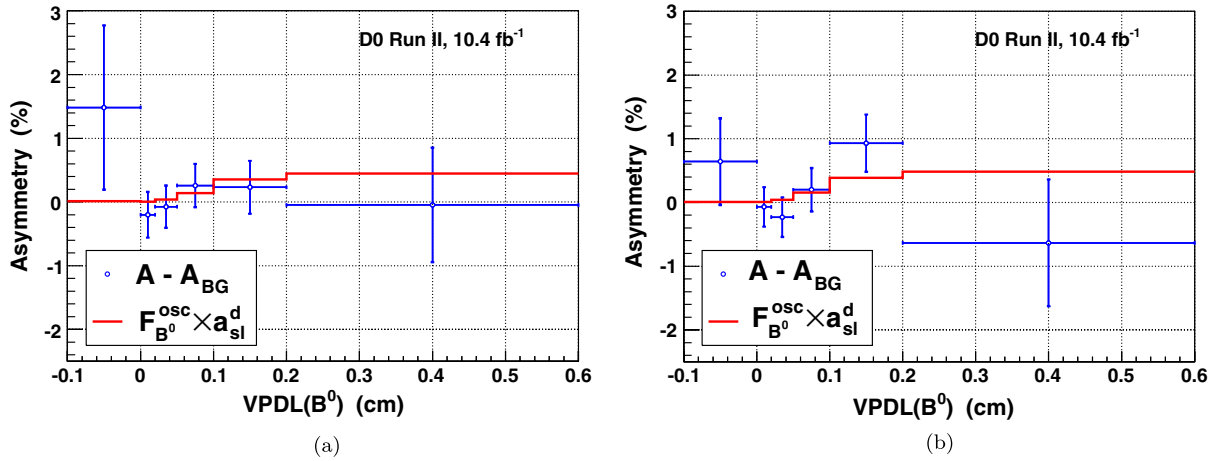

FIG. 8 (color online). Final measurements of the background corrected asymmetry, in bins of VPDL(B^0), for both channels. The points show the observed asymmetry, with the solid lines showing $F^{\rm osc}_{B^0} \cdot a^d_{\rm sl}$. Any asymmetry caused by mixing should exhibit a characteristic turn-on shape as the fraction of oscillated B^0 mesons increases. (a) μD channel; (b) μD^* channel.

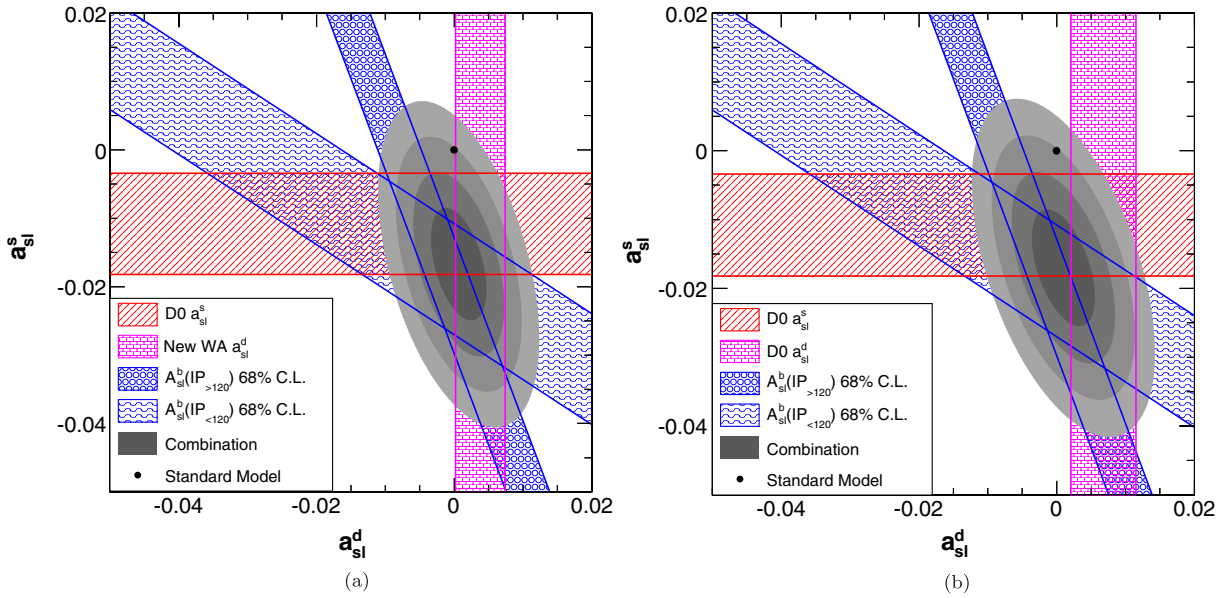

FIG. 9 (color online). Combination of measurements of $a^d_{\rm sl}$ (D0 and existing world average from B factories [6]), $a^s_{\rm sl}$ (D0 [31]), and the two impact-parameter-binned constraints from the same-charge dimuon asymmetry $A^b_{\rm sl}$ (D0 [19]). The bands represent the ± 1 standard deviation uncertainties on each measurement. The ellipses represent the 1, 2, 3, and 4 standard deviation two-dimensional confidence level regions of the combination. (a) Using a combination of D0 and B factory average for $a^d_{\rm sl}$; (b) Using the D0 value for $a^d_{\rm sl}$.

XI. COMBINATIONS WITH OTHER MEASUREMENTS

This measurement of $a^d_{\rm sl}$ can be combined with the existing world average from the B factories [6]. We use a simple weighted average, assuming that the two measurements are fully independent. The total uncertainty on the result presented in this article is $\pm 0.47\%$, obtained from the addition in quadrature of statistical and systematic uncertainties. The normalized weights are then 0.59 (D0) and 0.41 (WA). We obtain

$$a^d_{\rm sl} = (0.38 \pm 0.36)\%. \tag{45}$$

This number can in turn be combined with the recent $a^s_{\rm sl}$ measurement [31], and the two-dimensional constraints on $(a^d_{\rm sl}, a^s_{\rm sl})$ from the D0 measurement of the dimuon charge asymmetry $A^b_{\rm sl}$ [19]. The full two-dimensional fit yields the following values:

$$a^d_{\rm sl}({\rm comb}) = (0.07 \pm 0.27)\%, \tag{46}$$

$$a^s_{\rm sl}({\rm comb}) = (-1.67 \pm 0.54)\%, \tag{47}$$

where the two parameters have a correlation coefficient of -0.46. The results are shown in Fig. 9(a), with the two-dimensional contours overlaid on the four constraints from the input measurements. The fit returns a χ^2 of 2.0 for 2 degrees of freedom. The p value of the combination with respect to the SM point is 0.0037, corresponding to an inconsistency at the 2.9 standard deviation level.

Using only the D0 measurements of $a^d_{\rm sl}$, $a^s_{\rm sl}$, and $A^b_{\rm sl}$, we obtain the following values:

$$a^d_{\rm sl}({\rm comb}) = (0.10 \pm 0.30)\%, \tag{48}$$

$$a^s_{\rm sl}({\rm comb}) = (-1.70 \pm 0.56)\%, \tag{49}$$

with a correlation coefficient of -0.50. The χ^2 of this fit is 2.9, and the standard model p value is 0.0036, corresponding to a 2.9 standard deviation effect. Figure 9(b) shows the two-dimensional contours from this combination.

XII. CONCLUSIONS

We have performed a measurement of the semileptonic mixing asymmetry from B^0 decays, $a^d_{\rm sl}$, using $B^0 \to \mu^+ D^{(*)-} X$ decays in two independent channels. We obtain $a^d_{\rm sl} = [0.68 \pm 0.45({\rm stat}) \pm 0.14({\rm syst})]\%$, which is consistent with the SM prediction of $(-0.041 \pm 0.006)\%$. The resulting precision is dominated by limited statistics in the signal channel, and is better than the current world-average precision obtained by combining results from the B factories [Eq. (4)].

The background asymmetries are determined using data-driven methods in dedicated decay channels. The most important background is from differences in the reconstruction efficiencies for positively and negatively charged kaons, which is of order 1%. The use of simulation is limited to measuring the relatively small ($\sim$10%–20%) fraction of signal events which do not arise from B^0 decay, and modeling the oscillation of B^0 mesons.

ACKNOWLEDGMENTS

We thank the staffs at Fermilab and collaborating institutions, and acknowledge support from the DOE and NSF (USA); CEA and CNRS/IN2P3 (France); MON, Rosatom, and RFBR (Russia); CNPq, FAPERJ, FAPESP, and FUNDUNESP (Brazil); DAE and DST (India); Colciencias (Colombia); CONACyT (Mexico); NRF (Korea); FOM (The Netherlands); STFC and the Royal Society (United Kingdom); MSMT and GACR (Czech Republic); BMBF and DFG (Germany) ; SFI (Ireland); The Swedish Research Council (Sweden); and CAS and CNSF (China).

[1] A. D. Sakharov, Pis'ma Zh. Eksp. Teor. Fiz. **5**, 32 (1967) [Sov. Phys. Usp. **34**, 392 (1991)].
[2] M. S. Carena, J. M. Moreno, M. Quiros, M. Seco, and C. E. M. Wagner, Nucl. Phys. **B599**, 158 (2001).
[3] W. S. Hou, Chin. J. Phys. (Taipei) **47**, 134 (2009).
[4] S. Tulin and P. Winslow, Phys. Rev. D **84**, 034013 (2011).
[5] J. M. Cline, K. Kainulainen, and M. Trott, J. High Energy Phys. 11 (2011) 089.
[6] J. Beringer *et al.* (Particle Data Group), Phys. Rev. D **86**, 010001 (2012); http://www.slac.stanford.edu/xorg/hfag/osc/spring_2012/.
[7] P. Huet and E. Sather, Phys. Rev. D **51**, 379 (1995).
[8] A. Lenz and U. Nierste, J. High Energy Phys. 06 (2007) 072; Recent update arXiv:1102.4274.
[9] A. Lenz, U. Nierste, J. Charles, S. Descotes-Genon, A. Jantsch, C. Kaufhold, H. Lacker, S. Monteil, V. Niess, and S. T'Jampens, Phys. Rev. D **83**, 036004 (2011).
[10] B. H. Behrens *et al.* (CLEO Collaboration), Phys. Lett. B **490**, 36 (2000).
[11] D. E. Jaffe *et al.* (CLEO Collaboration), Phys. Rev. Lett. **86**, 5000 (2001).
[12] B. Aubert *et al.* (*BABAR* Collaboration), Phys. Rev. Lett. **92**, 181801 (2004).
[13] B. Aubert *et al.* (*BABAR* Collaboration), Phys. Rev. Lett. **96**, 251802 (2006).
[14] E. Nakano *et al.* (Belle Collaboration), Phys. Rev. D **73**, 112002 (2006).
[15] K. Ackerstaff *et al.* (OPAL Collaboration), Z. Phys. C **76**, 401 (1997).
[16] R. Barate *et al.* (ALEPH Collaboration), Eur. Phys. J. C **20**, 431 (2001).
[17] G. Abbiendi *et al.* (OPAL Collaboration), Eur. Phys. J. C **12**, 609 (2000).
[18] V. M. Abazov *et al.* (D0 Collaboration), Phys. Rev. D **74**, 092001 (2006).
[19] V. M. Abazov *et al.* (D0 Collaboration), Phys. Rev. D **84**, 052007 (2011).
[20] V. M. Abazov *et al.* (D0 Collaboration), Phys. Rev. D **85**, 032006 (2012).
[21] T. Aaltonen *et al.* (CDF Collaboration), Phys. Rev. D **85**, 072002 (2012); arXiv:1208.2967 [Phys. Rev. Lett. (to be published)].
[22] R. Aaij *et al.* (LHCb Collaboration), Phys. Rev. Lett. **108**, 101803 (2012).
[23] A. Lenz, U. Nierste, J. Charles, S. Descotes-Genon, H. Lacker, S. Monteil, V. Niess, and S. T'Jampens, Phys. Rev. D **86**, 033008 (2012).
[24] V. M. Abazov *et al.* (D0 Collaboration), Nucl. Instrum. Methods Phys. Res., Sect. A **565**, 463 (2006).
[25] R. Angstadt *et al.* (D0 Collaboration), Nucl. Instrum. Methods Phys. Res., Sect. A **622**, 298 (2010).
[26] G. Borisov, Nucl. Instrum. Methods Phys. Res., Sect. A **417**, 384 (1998).
[27] T. Sjöstrand, S. Mrenna, and P. Z. Skands, J. High Energy Phys. 05 (2006) 026.
[28] D. J. Lange, Nucl. Instrum. Methods Phys. Res., Sect. A **462**, 152 (2001).
[29] A. Hoecker *et al.*, Proc. Sci., ACAT2007 (**2007**) 040.
[30] V. M. Abazov *et al.* (D0 Collaboration), Phys. Rev. D **82**, 032001 (2010).
[31] V. M. Abazov *et al.* (D0 Collaboration), arXiv:1207.1769v1.